Chapter 1

Premixed Combustion in Spark Ignition Engines and the Influence of Operating Variables

Fabrizio Bonatesta

Additional information is available at the end of the chapter

http://dx.doi.org/10.5772/55495

1. Introduction

In the context of a Spark Ignition engine, the inherent complexity of premixed combustion is exacerbated by a range of engine variables that render the process highly transient in nature and not fully predictable. The present work aims to contribute to the continuous research effort to better understand the details of combustion and be able to model the process in gasoline SI engines. Coexisting fossil fuels depletion and environmental concerns, along with an alarming connection between traditional internal combustion engines emissions and human health degradation [1], have in recent years driven a strong research interest upon premixed SI combustion of energy sources alternative to gasoline, including liquid alcohols like ethanol, and gaseous fuels like hydrogen. However, the advancements enjoyed by gasoline-related technology and infrastructure in the last 40 years have eroded the potential advantages in efficiency and emissions offered by alternative fuels [2], and the SI engine running on gasoline continues to be the most common type of power unit used in passenger cars (Port-Fuel Injection gasoline engines accounted for the vast majority (91%) of all light-duty vehicle engines produced for the USA market in 2010 [3]).

The characteristics which make the gasoline engine well suited to light-weight applications include relatively high power to weight ratio, acceptable performance over a wide range of engine speeds, the vast infrastructure for gasoline and lower manufacturing costs when compared to diesel or more modern hybrid technologies [4]. The continuing exploitation of spark ignition engines reflects a history of successful development and innovation. These have included the electronic fuel injection system, exhaust emissions after-treatment, Exhaust Gas Recirculation and, increasingly, the use of some form of variable actuation valve train system. The modern SI engine, addressed to as high-degree-of-freedom engine by Prucka et al. [5], may also feature flexible fuel technology, typically to allow running on ethanol-gasoline blended fuels.

As the technology advances, the number of engine actuators increases and so does the number of variables that may potentially modify the combustion process. Methods of combustion control based on look-up tables may well be implemented in *high-degree-of-freedom* engines, for example to set optimal spark timing and phase combustion appropriately across Top Dead Centre, but are not well-suited during transient operation, when the boundary conditions are changing on a cycle-to-cycle basis. Whilst controlling the combustion process in highly complex engine architectures becomes more challenging, the development of straightforward modelling approaches, which allow reliable inclusion within real-time feed-forward engine controllers become essential to ensure improved performance and fuel efficiency also during transient or variable operation.

The premixed, homogeneous charge gasoline combustion process in SI engines is influenced by the thermo-chemical state of the cylinder charge. Significant factors are local temperature and pressure, stoichiometry and the contents of burned gas within the combustible mixture; these quantities affect rate of burning and consequent in-cylinder pressure development. The combustion process is also greatly influenced by cylinder bulk motion and micro-scale turbulence. Understanding the connection between charge burn characteristics and relevant engines operating variables in the context of modern technologies is extremely useful to enable and support engine design innovation and the diagnosis of performance. The present chapter explores the evolution of the combustion process in modern-design gasoline engines, as indicated by the cylinder charge Mass Fraction Burned variation and combustion duration, and the most relevant factors influencing these. It also explores the use, accuracy and limitations of recently-proposed empirical, non-dimensional (or simplified thermodynamic) combustion models which respond to the requirements of fast execution within model-based control algorithms, and discusses relevant results, which entail the use of Variable Valve Timing systems. An exemplar simplified quasi-dimensional models is also presented at the end of the chapter, along with some relevant results concerning an application to flexible fuel, gasoline/ethanol operation. All the experimental data and models discussed here refer and are applicable to stable combustion, typically identified by a Coefficient of Variability of the Indicated Mean Effective Pressure (CoV of IMEP) smaller or equal to 6% [6]. Although the importance of cycle-by-cycle variability is acknowledged, as this may arise from highly diluted combustion, the topic of unstable combustion has not been the focus of the present work.

2. Premixed combustion in SI engines

The present section reviews important features of the premixed combustion process in SI engines, introducing basic terms and definitions of relevant variables and combustion indicators. Ample space is dedicated to the working principles of VVT systems and how these may fundamentally affect the combustion process. This section ultimately provides definitions and methods of determination of in-cylinder charge diluent fraction, as the one most influential variable on combustion strength, duration and stability, in the case of engines fitted with a VVT system.

http://dx.doi.org/10.5772/55495

2.1. Overview of flame propagation mechanism

Detailed observations of development and structure of the flame in SI engines can be made by using direct photographs or other methods such as Schlieren and shadowgraph photography techniques [6, 7]. The initial stage of the combustion process is the development of a flame kernel, centred close to the spark-plug electrodes, that grows from the spark discharge with quasi-spherical, low-irregular surface; its outer boundary corresponds to a thin sheet-like developing reaction front that separates burned and unburned gases. Engine combustion takes place in a turbulent environment produced by shear flows set up during the induction stroke and then modified during compression. Initially, the flame kernel is too small to incorporate most of the turbulence length scales available and, therefore, it is virtually not aware of the velocity fluctuations [8]. Only the smallest scales of turbulence may influence the growing kernel, whereas bigger scales are presumed to only convect the flame-ball bodily; the initial burning characteristics are similar to those found in a quiescent environment (a laminar-like combustion development). As the kernel expands, it progressively experiences larger turbulent structures and the reaction front becomes increasingly wrinkled. During the main combustion stage, the thin reaction sheet becomes highly wrinkled and convoluted and the reaction zone, which separates burned and unburned gases, has been described as a *thick turbulent flame brush*. While the thickness of the initial sheet-like reaction front is of the order of 0.1 mm, the overall thickness of this turbulent flame brush can reach several millimetres; this would depend on type of fuel, equivalence ratio and level of turbulence. The turbulent flow field, in particular velocity fluctuations, determines a conspicuous rate of entrainment in the reaction zone, which has been described [9, 10] as being composed of many small pockets and isolated island of unburned gas within highly marked wrinkles that characterize a thin multi-connected reaction sheet. Theories have been advanced that describe the local boundary layer of this region as a quasi-spherical flame front, which diffuses outwards with laminar flame speed [6].

Gillespie and co-workers provide a useful review of those aspects of laminar and turbulent flame propagation, which are relevant to SI engines combustion [8]. Similarly to laminar-like combustion taking place in a quiescent environment, two main definitions of time-based combustion rate can be proposed for turbulent combustion. The first one relates to the rate of formation of burned products:

$$\frac{dm_b}{d\tau} = \rho_u \; A_f \; S_b \tag{1}$$

The second one considers the rate of mass entrainment into the flame-front:

$$\frac{dm_e}{d\tau} = \rho_u \; A_f \; S_e \tag{2}$$

In the above fundamental expressions of mass continuity, ρ_u is the unburned gas density, A_f is a reference reaction-front surface area and S_b (or S_e) is the turbulent burning (or entrainment)

velocity. The dependence of the combustion rate on turbulence is embodied in the velocity term, which is fundamentally modelled as a function of turbulence intensity, u', and laminar burning velocity, S_L. The latter, loosely addressed to as laminar flame velocity in the context of simplified flame propagation models, has been demonstrated to retain a leading role even during turbulent combustion and depends strongly upon the thermodynamic conditions (namely pressure and temperature) and upon the chemical state (namely combustible mixture strength, i.e. stoichiometry, and burned gas diluent fraction) of the unburned mixture approaching the burning zone.

The difference between the two expressions of the combustion rate depends on the real, finite flame front thickness that at each moment in time would host a certain mass $(m_e - m_b)$, already entrained into the reaction zone but not yet burned. Several definitions can be used for the reference surface-area: the quantity A_f identified above is the stretched cold flame-front, usually assumed to be smooth and approximately spherical, detectable with good approximation using Schlieren images techniques and then traced with best-fit circles [11, 12]. A different approach considers the so-called burning surface A_b, defined as the surface of the volume V_b that contains just burned gas: the difference $(r_f - r_b)$ between the correspondent radii would scale with the size of the wrinkles that characterise the real, thick reaction zone. When the burning velocities are calculated from experimental burning rates/pressure data (see below), the cold surface A_f is often equated to the burning surface A_b [13], which assumes that the thickness of the reaction zone/front-sheet can be neglected.

Flame sheets, in real combustion processes, are subject to stretch, which shows a smoothing effect on the flame-front surface, and tends to reduce the burning velocities. When the flame is fully developed, incorporating most of the available turbulent spectrum, geometrical stretch is superseded by aerodynamic strain. The action of flame stretching in all stages of combustion reduces at increasing pressure, being low at engine-like operating conditions [8].

2.2. In-cylinder motion field and effects on combustion

Although the mean charge velocity in an engine cylinder may have an effect on the initial rate of combustion, by distorting the developing flame kernel and, possibly, by increasing the available burning surface [14], the main mechanism of combustion enhancement is turbulence.

Modern-design gasoline engines typically have 4 valves per cylinder, 2 intake and 2 exhaust valves. The use of two intake valves, which gives symmetry of the intake flow about the vertical axis, generates a mean cylinder motion called tumble, or vertical or barrel swirl, an organised rotation of the charge about an axis perpendicular to the cylinder axis. The strength of a tumbling flow is measured by means of a non-dimensional number called tumble ratio, defined as the ratio between the speed of the rotating bulk-flow and the rotational speed of the engine. The tumbling mean flow has been observed to promote combustion [15, 16] through turbulence production towards the end of the compression stroke. As the flow is compressed in a diminishing volume, the rotating vortices that make up the tumbling flow tend to break down into smaller structures and their kinetic energy is gradually and partially converted in turbulent kinetic energy. Whether the turbulence intensity is actually rising during compres-

http://dx.doi.org/10.5772/55495

sion (and at the start of combustion) would be dictated by the concurrent rates of turbulence production and natural viscous dissipation [17]. Although the literature is somewhat unclear on this specific topic, increased tumble ratio has been also reported to improve the cyclic stability and extend the running limits for lean or diluted mixtures [15, 18].

Two parameters are commonly used to describe the effects of turbulence on flame propagation: integral length scale L and turbulence intensity u'. The first one is a measure of the size of the large turbulent eddies and correlates with the available height of the combustion chamber; when the piston is at TDC of combustion, L is typically 2 mm [19]. The second parameter is defined as the root-mean-square of the velocity fluctuations. According to numerous experimental studies available in the literature, for example [12, 20, 21], the turbulence intensity, for given engine and running set-up, would depend primarily on engine speed (or mean piston speed). Computational Fluid Dynamics studies of the in-cylinder turbulence regime, performed by the Author [22] on a PFI, 4-valve/cylinder, pent-roof engine show that turbulence intensity (modelled using a conventional $k-\varepsilon$ approach [6]) is characterised by a weakly decreasing trend during compression and up to TDC of combustion. In the range of engine speeds investigated, which were between 1250 and 2700 rev/min, the volume-averaged value of turbulence intensity, when piston is approaching TDC, can be approximated by the correlation: $u' \approx 0.38 S_P$, where S_P is the mean piston speed (units of m/s), given by $S_P = 2SN$, with S engine stroke (m) and N engine speed (rev/s).

Theories have been developed which ascribe importance to additional turbulence generated inside the unburned region ahead of the reaction-front, by the expanding flame. None of them has been confirmed by direct observations and their validity has been always inferred by means of comparisons between models predictions and experimental data. Tabaczynski and co-workers [23, 24] advance the so-called eddy rapid distortion theory according to which the individual turbulence eddies experience fast isentropic compression, in such a way that their angular momentum is conserved. They conclude that due to this interaction the turbulence intensity increases and the length scale reduces, respectively, during the combustion process. Hoult and Wong [25], in a theoretical study based on a cylindrical constant-volume combustion vessel, apply the same rapid distortion theory to conclude that the turbulence level of the unburned gas depends only on its initial value and the degree of compression due to the expanding flame. An interesting fit of experimental data to inferred combustion-generated turbulence intensity is due to Groff and Matekunas [12].

2.3. Variable valve actuation mechanisms

The most commonly stated reason for introducing Variable Valve Actuation systems in SI engines is to raise the engine brake torque and achieve improvements in its variation with engine speed, especially at low speed (including idle conditions) and at the high end of the engine speed range. A second coexistent reason is to reduce the exhaust emissions, especially nitrogen oxides, but also unburned hydrocarbons [26]. Today many modern engines are equipped with VVA technology because measurable improvements can be gained in fuel consumption and efficiency over wide ranges of operating conditions, including part-load conditions. Efficiency improvements are a direct consequence of a reduction in pumping (intake throttling) losses. At

low to medium load, variable valve strategy, in particular the extension of the valve overlap interval (between the Intake Valve Opening and Exhaust Valve Closing), exerts a strong influence upon the amount of burned gas recirculated from one engine cycle to the following one. This amount, or more specifically the so-called dilution mass fraction, has a profound influence upon combustion rates and duration. Combustion control strategies which aim at improved efficiency across the whole range of engine speeds and loads must carefully consider the extent to which the burning characteristics may be modified by VVA.

2.3.1. Overview of VVA mechanisms

The development of VVA mechanisms started in the late 1960s and the first system was released into production in 1982 for the USA market, prompted by tightening emissions legislation [26]. The mechanism was a simple two-position device, which reduced the valve overlap at idle conditions, improving combustion stability and hence reducing the noxious emissions. Very different objectives, in particular the increase of the brake torque output at both ends of the engine speed range, induced a second manufacturer to develop a VVA system for small-capacity motorcycle engines. Released also in the early 1980s, the system worked by simply deactivating one inlet and one exhaust valve per cylinder at engine speeds below a fixed limit, achieving better mixing and greater in-cylinder turbulence as the available inlet flow area was reduced. A better understanding of the potential advantages in fuel efficiency has prompted, in recent years, an increased interest in VVA technology and most major manufacturers now produce engines with some form of VVA. Most systems presently in use allow continuous variable camshaft phasing; some complicated mechanisms are capable of switching cams to gain the benefits of different valve lifting profiles. From 2001 at least one manufacturer incorporated a variable valve lift and phase control mechanism into the first production engine that featured throttle-less control of engine load [27]. The amount of fresh air trapped into the cylinder is controlled solely by appropriate Intake Valve Closing strategy, removing the need for throttling and the associated pumping losses. Variable lift serves as a means of controlling the air induction velocity and ultimately the level of in-cylinder turbulence.

Ahmad and co-workers [28] classify the VVA systems into five categories depending on their level of sophistication. The most complicated devises are classified in category 5, capable of varying valve lift, opening durations and phasing, independently of each other for both intake and exhaust valve trains. Despite the potential advantages, mechanical systems in category 5 tend to be expensive, physically bulky and complicated. The mechanism used by the Author for the experimental work reported in the following sections is classified in category 3, as it allows continuous and independent variable phasing of intake and exhaust valve opening intervals, with fixed valve lifting profiles. This system is usually called Twin Independent-Variable Valve Timing. The Twin Equal-VVT system represents a simplification of the TI-VVT, where both camshafts are phased simultaneously by equal amounts.

2.3.2. VVT strategies and influence on charge diluent fraction

By means of multiple combinations of intake and exhaust valve timings, the TI-VVT system allows the identification of optimal operating strategies across the whole range of engine

http://dx.doi.org/10.5772/55495

speed and load operating conditions. Early Intake Valve Opening timings produce large valve overlap interval and increase charge dilution with burned gas. Late IVO timings lead to increased pumping work, but may show an opposite effect at high engine speed where volumetric efficiency gains can be achieved by exploiting the intake system ram effects [6]. If the valve motion profiles are fixed, changes to IVO are reproduced by those to IVC, with significant effects on mass of fresh charge trapped, hence on engine load, and measurable changes in pumping losses. Early IVC controls engine load by closing the inlet valve when sufficient charge has been admitted into the cylinder. Reductions in Brake Specific Fuel Consumption of up to 10% have been observed with early IVC strategies [29, 30]. Recent studies by Fontana et al. [31] and by Cairns et al. [32] show similar reductions in fuel consumption, but explain these referring to the *displacement* of fresh air with combustion products during the valve overlap interval, which reduces the need for throttling. The Exhaust Valve Opening strategy would be dictated by a compromise between the benefits of the exhaust blow-down (early EVO) and those associated to a greater expansion ratio (late EVO). At high speed and load conditions, late EVC exploits the benefits of the ram effect, which may assist in the combustion products scavenging process. The exhaust valve strategy also contributes to the process of *mixture preparation* at all engine conditions, by trapping burned gases in the cylinder (early EVC) or by backflow into the cylinder when intake and exhaust valves are overlapping (late EVC).

Focusing on preparation of the combustible mixture and subsequent combustion process, the level of charge dilution by burned gas is the single most influential quantity, which is heavily varied using variable valve timing. Charge dilution tends to slow down the rate of combustion by increasing the charge heat capacity, ultimately reducing the adiabatic flame temperature. Charge dilution tends to increase with increasing valve overlap, particularly under light-load operating conditions when intake throttling produces a relatively high pressure differential between the exhaust and intake manifolds. This promotes a reverse flow of exhaust gas into the cylinder and intake ports. The recycled gas forms part of the trapped charge of the following engine cycle. There is a strong degree of interaction between the level of combustion products within the newly formed mixture and engine speed and load. Increasing speed shortens the duration of the valve overlap in real time, while increasing load raises the pressure-boundary of the intake system limiting the recirculating hot flows. At high speed and load conditions the increase of charge dilution with increasing valve overlap is limited.

2.4. Charge dilution mass fraction – Definitions and measurements

In the case of a gasoline engine fitted with VVT system, the dilution mass fraction is the sum of two different terms. The first one, properly named residual gas fraction, is associated with the amount of burned gas remaining inside the combustion chamber when the piston reaches the TDC of the exhaust stroke. If the exhaust valve closes before TDC, then the residual mass fraction would be given by the amount of burned gas trapped inside the cylinder at EVC. In symbols, the residual mass fraction is written as:

$$x_r = \frac{m_r}{m_{tot}} \tag{3}$$

The second term is the Internal-Exhaust Gas Recirculation, i.e. the amount of burned gas recirculated from the exhaust port to the intake while the valves are overlapping. The associated gas fraction is:

$$x_{IEGR} = \frac{m_{IEGR}}{m_{tot}} \tag{4}$$

Since there are no physical ways to distinguish between m_r and m_{IEGR}, the total mass of spent gas recycled from one engine cycle to the following one is simply referred to as burned mass, m_b. The total dilution mass fraction assumes the form:

$$x_b = \frac{m_r}{m_{tot}} + \frac{m_{IEGR}}{m_{tot}} = \frac{m_b}{m_{tot}} \tag{5}$$

In the previous expressions, m_{tot} is the total mass trapped inside the cylinder at IVC, given by the addition of all the single contributions to the total:

$$m_{tot} = m_{fuel} + m_{air} + m_b \tag{6}$$

The total cylinder mass should also account for a small but not negligible mass of atmospheric water vapor, which can be safely assumed to be a constant fraction of m_{air}.

2.4.1. Measurements of dilution

Methods to measure the cylinder charge diluent fraction are usually divided into two main categories: invasive or *in situ* techniques, and non-invasive. Invasive techniques, such as Spontaneous Raman Spectroscopy and Laser Induced Fluorescence, require physical modifications to the engine, likely interfering with the normal combustion process [33]. The experimental data presented in the following sections have been collected using a non-invasive in-cylinder sampling technique, which entails the extraction of a gas sample during the compression stroke of every engine cycle, between IVC and Spark Timing. The small extracted gas stream, controlled via a high-frequency valve, is passed through a first GFC IR analyser, which can work reliably at low flow rates, to yield carbon dioxide molar concentrations within the cylinder trapped mass. A second GFC IR analyser is used to measure exhaust CO_2, at the

http://dx.doi.org/10.5772/55495

same time. Dilution mass fraction is calculated exploiting the readings from the two analysers, with the expression:

$$x_b = \frac{m_b}{m_{tot}} = \frac{\left(\tilde{x}_{CO2}\right)_{compr} - \left(\tilde{x}_{CO2}\right)_{air}}{\left(\tilde{x}_{CO2}\right)_{exh} - \left(\tilde{x}_{CO2}\right)_{air}} \tag{7}$$

In equation (7), $\left(\tilde{x}_{CO2}\right)_{compr}$ is mole fraction of CO_2 in the unburned mixture extracted during compression; $\left(\tilde{x}_{CO2}\right)_{exh}$ is the mole fraction in the exhaust stream, and $\left(\tilde{x}_{CO2}\right)_{air}$ refers to the fresh intake air (this can be assumed constant at 0.03%). A full derivation of equation (7), along with validation and experience of use of the cylinder charge sampling system, can be found in [22] and in [33].

Since CO_2 is normally measured in fully dried gas streams, the outputs from the analysers are dry mole fractions and need to be converted into wet mole fractions to obtain real measurements. Heywood [6] suggests using the following expression for the correction factor:

$$K = \frac{\tilde{x}_i}{\tilde{x}_i^*} = \frac{1}{1 + 0.5\left[\left(m/n\right)\left(\tilde{x}_{CO2}^* + \tilde{x}_{CO}^*\right) - 0.74\left(\tilde{x}_{CO}^*\right)\right]} \tag{8}$$

In equation (8), $\tilde{x}_i^*$ indicates dry mole fractions of the i-th component, while $(m/n)=1.87$ is the hydrogen to carbon ratio of the gasoline molecule. The K factor assumes different values if calculated using in-cylinder samples or exhaust stream ones, hence separate calculations are necessary. Data collected during the present research work show that, independently of the running conditions, wet dilution levels are 11% to 13% greater than dry dilution levels.

2.4.2. Dilution by external exhaust gas recirculation

In an engine fitted not only with VVT system, but also with External-Exhaust Gas Recirculation system, the total mass of spent gas trapped at IVC accounts for a further source ($m_b = m_r + m_{IEGR} + m_{EEGR}$), and the total dilution is written as:

$$x_b = \frac{m_r}{m_{tot}} + \frac{m_{IEGR}}{m_{tot}} + \frac{m_{EEGR}}{m_{tot}} = \frac{m_b}{m_{tot}} \tag{9}$$

The externally recirculated gas is commonly expressed as a fraction (or percentage) of the intake manifold stream. The formulation which allows the calculation of this quantity is:

$$EEGR = \frac{\dot{m}_{EEGR}}{\dot{m}_{man}} = \frac{\left(\tilde{x}_{CO2}\right)_{man} - \left(\tilde{x}_{CO2}\right)_{air}}{\left(\tilde{x}_{CO2}\right)_{exh} - \left(\tilde{x}_{CO2}\right)_{air}} \tag{10}$$

Symbols in the above expression retain the same meaning as before; $(\tilde{x}_{CO2})_{man}$ is the molar concentration of carbon dioxide in the intake manifold stream. The correlation connecting the total in-cylinder dilution and the dilution from External-EGR can be easily derived:

$$x_{EEGR} = \frac{m_{EEGR}}{m_{tot}} = \frac{\left(1 - x_b\right)\ EEGR}{1 - EEGR} \tag{11}$$

3. Combustion evolution: The mass fraction burned profile

The evolution of the combustion process as indicated by the MFB variation is considered in the present section. Two methods of deriving this variation from measurements of Crank Angle resolved in-cylinder pressure are normally used. These are the Rassweiler and Withrow method or its variants [34, 35] and the application of the First Law of the Thermodynamics. The two approaches have been shown to yield closely comparable results in the case of stable combustion [22]. The Rassweiler and Withrow method and its inherent limitations are the main focuses here. All the experimental data presented in this section and in the following ones refer to the same research engine, unless otherwise specified. Technical specifications of this engine are given in section 4.1.

The quantity so far addressed to as MFB, is a non-dimensional mass ratio that can be expressed as:

$$\left[x_{MFB}\right]_\tau = \frac{\left[m_b\right]_\tau}{m_{fc}} \tag{12}$$

Here, $[m_b]_\tau$ is the mass actually burned at any instant τ after combustion initiates and m_{fc} is the mass of fresh charge, including air and fuel, trapped inside the engine cylinder at IVC. Plotted as function of CA, the MFB profile assumes a characteristic S-shape, from 0% at ST to 100% when combustion terminates. Figure 1 shows the in-cylinder pressure trace for a firing cycle, the corresponding MFB profile and the motored pressure trace collected at the same engine speed and throttle valve setting.

During the early flame development, that in the case of figure 1 begins with the spark discharge at 26 CA degrees BTDC, the energy release from the fuel that burns is so small that the pressure rise due to combustion is insignificant; firing and motoring pressure traces are, therefore, coincident. During this period, over about 13 CA degrees, the MFB rises very slowly. At the

http://dx.doi.org/10.5772/55495

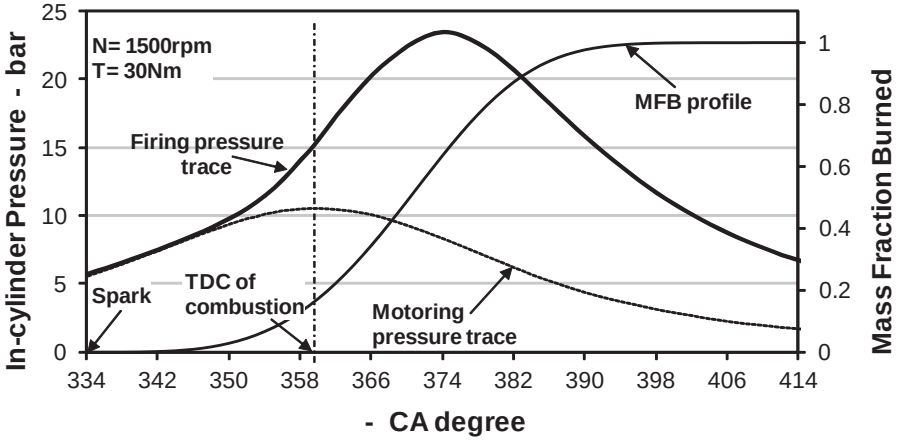

Figure 1. In-cylinder pressure trace for a firing cycle (bold line) and corresponding MFB profile (fine line); operating condition: engine speed N = 1500 rev/min; engine torque output T = 30 Nm. Dashed line represents the pressure trace for the motored cycle.

end of this stage an amount of charge as small as 1% has burned. During the second phase, the chemical energy release, from a stronger rate of burning, gives rise to the firing-cycle pressure trace. After peak pressure, that falls in this case at 15 CA degrees ATDC, when there is already an extensive contact between flame surface and cylinder walls, the MFB approaches 100% with progressively decreasing slope.

The MFB profile provides a convenient basis for *combustion characterisation*, which divides the combustion process in its significant intervals, flame development, rapid burning and combustion termination, in the CA domain. The initial region of the curve, from the spark discharge to the point where a small but identifiable fraction of the fuel has burned, represents the period of flame development. It is common to find the Flame Development Angle defined as the CA interval between ST and 10% MFB:

$$FDA = \vartheta_{10\%} - \vartheta_{ST} \tag{13}$$

FDA covers the transition between initial laminar-like development and the period of fast burning where the charge burns in quasi-steady conditions, i.e. with a fairly constant mass flow rate through the thick reaction-front [9]. An alternative definition of the FDA, as the interval between ST and 5% MFB, is also common. Other definitions which refer to a shorter development interval (e.g. ST to 1% MFB) suffer from inaccuracies due to the low gradient of the MFB profile during the initial phase of the process.

The following combustion interval, the Rapid Burning Angle, is typically defined as the CA interval during which the MFB rises between 10% and 90%:

$$RBA = \vartheta_{90\%} - \vartheta_{10\%} \tag{14}$$

The selection of 90% MFB as limiting point is dictated by convenience since the final stage of combustion is difficult to identify. During the so-called combustion termination the chemical energy release from the fuel that burns is comparable to other heat transfer processes that occur at the same time; during this stage the MFB increases only slightly over a large number of CA degrees.

3.1. The rassweiler and withrow method

In the present section and in the following ones, the Rassweiler and Withrow method has been used for MFB calculations from ensemble-averaged experimental pressure records and volume variation data. The method is well established due to ease of implementation, which allows real-time processing and because it shows good intrinsic tolerance to pressure signal noise across wide ranges of engine operating conditions [35]. Its rationale comes from observations of constant-volume bomb explosions, where the fractional mass of burned charge has been seen to be approximately equal to the fractional pressure rise. If P_{tot} and $[P]_\tau$ are, respectively, pressure at the end of combustion and at a generic time τ , this equality can be written as:

$$\left[x_{MFB}\right]_\tau = \frac{\left[m_b\right]_\tau}{m_{fc}} \approx \frac{\left[P\right]_\tau}{P_{tot}} \tag{15}$$

More precisely, the pressure rise due to combustion is proportional to chemical heat release rather than to fractional burned mass, but MFB calculations using the above approximation are consistently in agreement with those from thermodynamic models [36].

In order to apply to engine-like conditions the analogy with constant-volume bombs, the total pressure rise measured across a small CA interval is divided into contributions due only to combustion and only to volume variation:

$$\Delta P = \Delta P_c + \Delta P_V \tag{16}$$

In each CA step, increments due to piston motion are calculated assuming that pressure undergoes a polytropic process:

$$\left[\Delta P_V\right]_{\vartheta \to \vartheta+1} = P_\vartheta \left[\left(\frac{V_\vartheta}{V_{\vartheta+1}}\right)^n - 1\right] \tag{17}$$

http://dx.doi.org/10.5772/55495

Constant-volume bomb experiments have also shown that the pressure increment due to combustion, the total mass being constant, is inversely proportional to volume. In order to draw a second analogy with engine combustion, the combustion pressure rise at each step, calculated as $(\Delta P - \Delta P_V)$, is multiplied by a volume ratio which eliminates the effects of volume changes. The relation:

$$\left[\Delta P_c\right]_{\vartheta \to \vartheta+1} = \left[\Delta P - \Delta P_V\right]_{\vartheta \to \vartheta+1} \frac{V_\vartheta}{V_{ref}} \tag{18}$$

allows determining the pressure increments due to combustion as if they all occur into the same volume V_{ref} . The reference volume is taken equal to the clearance volume, i.e. the combustion chamber volume when the piston is at TDC. The relation that gives the MFB as a function of CA is finally obtained:

$$\left[x_{MFB}\right]_\vartheta = \sum_{\vartheta_{ST}}^{\vartheta} \Delta P_c \quad / \quad \sum_{\vartheta_{ST}}^{EOC} \Delta P_c \tag{19}$$

EOC indicates the CA location of End Of Combustion, corresponding to 100% MFB.

3.1.1. Polytropic indexes and EOC condition for MFB calculation

The method discussed above provides a robust platform to extract combustion evolution information from sensors data which are routinely acquired. Nevertheless, its accuracy is questionable as necessary constrains such as the EOC are not easily identifiable, and because it accounts for heat losses to the cylinder walls only implicitly, by selecting appropriate polytropic indices for compression and expansion strokes.

In theory, the polytropic index which figures in equation (17) should change continuously during combustion. However, this is not practical and an easier strategy of indices determination must be adopted. In the work presented here, two different values of the polytropic index are used for intervals in the compression and power strokes, respectively. The evaluation of the MFB curve proceeds by successive iterations, until appropriate values of the polytropic indexes, in connection with the determination of EOC, are established. The sensitivity of pressure increments to these indices increases with pressure and then is emphasized after TDC, when the in-cylinder pressure reaches its maximum. While the sensitivity of the MFB profile to the compression index is relatively low, the selection of the expansion index is more important. During compression the unburned mixture roughly undergoes a polytropic process that begins at IVC. In this work the polytropic compression index is calculated as the negative of the slope of the experimental [log V, log P] diagram over 30 consecutive points before ST, and maintained unvaried up to TDC. During the expansion stroke the polytropic index varies due to several concurrent phenomena, including heat transfer, work exchange and turbulence variation. In theory, it increases approaching an asymptotic value just before EVO. As

suggested by Karim [37], the EOC associates the condition $\Delta P_c = 0$ with an expansion index which settles to an almost constant value. Provided a reasonable condition is given to determine the EOC, the correct expansion index would be the one that, when combustion is over, maintains the MFB profile steadily at 100% till EVO: *the zero combustion-pressure condition* [35]. In this work, the expansion index is estimated with an iterative procedure where, starting from a reference value (e.g. 1.3), the index is progressively adjusted together with the EOC, until the MFB profile acquires a *reasonable* S-shape, which meets the requirement of the zero combustion-pressure condition. Several methods are reported in the literature to determine the EOC; the first negative and the sum negative methods, for example, assume that EOC occurs when one or three consecutive negative values of ΔP_c are found. In this work, the combustion process is supposed to terminate when ΔP_c becomes a negligible fraction (within 0.2%) of the total pressure increment ΔP for 3 CA-steps consecutively.

3.1.2. Other methods of estimation of the expansion index

Other methods have been proposed for the evaluation of $n_{\exp}$. One calculates the index as the slope of the log-log indicator diagram over narrow intervals before EVO. Although this approach avoids the EOC determination, experimental results show that the calculations are sensitive to the chosen interval and, in general, combustion duration is overestimated. As an improvement to this method, $n_{\exp}$ has been calculated as the value that gives average ΔP_c equal to zero after combustion terminates, satisfying the zero combustion-pressure condition [35]. Again, this approach seems to be sensitive to the interval over which the average ΔP_c is evaluated, reflecting pressure measurements noise and the fact that often $n_{\exp}$ does not settle properly before EVO. Figure 2 directly compares three different methods of expansion index determination for engine speed of 1900 rev/min and torque of 40 Nm (similar results are obtained at different operating conditions): with the view that the iterative method of $n_{\exp}$ estimate yields accurate MFB characteristics (which, for stable combustion, are consistently similar to those from thermodynamics models [22]), the modification proposed in [35] tends to overestimate combustion duration during the rapid stage and especially during the termination stage, with the effect of delaying the EOC. The method for estimating the expansion index is crucially important as different methods may cause over 40% variation in the calculated RBA.

3.2. Estimated errors in the MFB profile

The calculated burning characteristics of an engine, including the MFB profile, may be affected by measurements and calculation errors. Most of the potential inaccuracies are associated with the determination of the absolute in-cylinder pressure. The adoption of ensemble-averaged pressure trace, which as in the present work should be based on the acquisition of a minimum of 100 individual cycles [38], is beneficial to diminish the cyclical dispersion errors (inter-cycle pressure drift) [39] and signal noise. The major source of cylinder pressure error is indeed associated with thermal-shock and can be accounted for in terms of short-term or intra-cycle pressure drifts. Pressure sensors do not measure absolute pressure and the sensor signal need

http://dx.doi.org/10.5772/55495

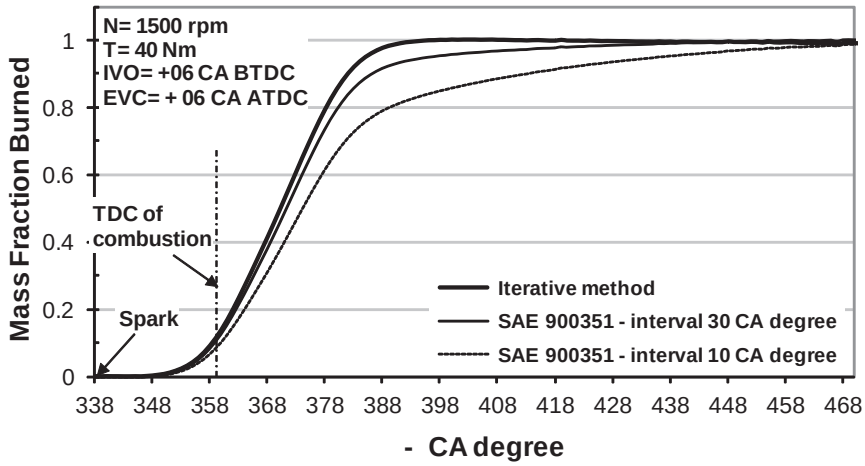

Figure 2. MFB profiles built using three different methods of expansion index evaluation.

referencing to a known value. Since thermal-shock is driven by combustion, it would be preferable to perform cylinder pressure referencing when the artificial variability due to temperature changes is at a minimum, a circumstance which is likely to occur at the end of the intake stroke [40]. Nevertheless, the thermally induced drift persists throughout the whole engine cycle, assigning uncertainty to the experimental measurements. Payri et al. [39] account for a value of pressure accuracy of ±0.15 bar, estimated as maximum pressure difference at BDC of induction. Studies carried out by the Author [22] have shown that a value of intra-cycle pressure drift (calculated as difference between transducer BDC outputs at the beginning and at the end of single cycles) of ± 0.1 bar (with standard deviation of 0.055 bar) represents a realistic average estimate of the potential inaccuracy of the in-cylinder pressure.

When MFB profiles are built applying the Rassweiler and Withrow method to ensemble-averaged in-cylinder pressure records, at least two sources of errors can be considered: pressure measurements inaccuracy, but also the consequential polytropic compression index variation. Expansion index and EOC location are also affected by pressure variation but, if the iterative optimisation technique described above is used, these cannot be enumerated among the causes of uncertainties. The compression index variation is a linear function of the pressure variation at BDC of induction, almost independently of engine speed and load. A variation of +10% in BDC pressure induces a reduction of the compression index of about -1.5% [22]. Further studies on the effects of pressure drift (used as an offset) on the MFB profile, have shown that the region mostly affected is the flame development interval between ST and 10% MFB. For a pressure offset of ±0.1 bar, typical values of MFB percentage variation are likely to be around ±6% at 10% MFB for low engine load (IMEP = 2.5 bar); the error reduces proportionately at increasing load (typically ±1.5% at 10% MFB for IMEP = 6 bar). After 10% MFB, the

MFB variation reduces consistently, reaching very small values, perhaps 1% or 0.5%, at 90% MFB. The error study by Brunt et al. [41] shows similar nature and magnitude of errors.

4. The effects of operating variables on combustion

The strength and duration of combustion in a given engine depend on a range of operating variables and, as stated in the beginning, the number of these tends to increase as technology advances. Understanding the connection between operating variables and burn rate characteristics is fundamental as the latter govern pressure development, spark timing requirements and, ultimately, work output and engine efficiency. The present section explores the results of an experimental research work carried out by the Author with the aim of enhancing the knowledge of how engine variables influence the progression of combustion in a modern engine featuring VVT system [42]. Conditions investigated covered light to medium engine load and speed, representative of urban and cruise driving conditions.

4.1. Experimental methodology

The test engine used in this work is a 1.6 litres, 4-cylinder, 4-valve/cylinder, PFI, SI engine, fitted with independent intake and exhaust valve timing control (TI-VVT) and central spark, pent-roof combustion chamber geometry. The technical details of the engine are summarised in Table 1. Engine testing was carried out under fully-warm, steady-state operating conditions and combustion was always kept stoichiometric, a requirement for high efficiency of 3-way catalytic convertors under most operating conditions. The air-to-fuel ratio was measured using a universal exhaust gas oxygen sensor and checked carrying out carbon and oxygen balances on the exhaust gases. The fuel used was grade 95 RON gasoline. Running conditions covered engine speed between 1500 and 3500 rev/min, IMEP between 2 and 7 bar, and spark ignition timing between 35 and 8 CA degrees BTDC.

The valve overlap, which controlled the diluent fraction via internal-EGR, was changed either by changing the EVC at constant IVO timing, or by changing the IVO at constant EVC timing. Timings here, as in the rest of the chapter, are given in terms of Crank (not Cam) Angles. The default EVC timing was +6 CA degrees ATDC, and the default IVO timing was +6 CA degrees BTDC. EVC sweeps covered the range -14 to +36 CA degrees ATDC, whereas IVO sweeps covered the range -24 to 36 CA degrees BTDC. The resulting overlap intervals varied from -20 (negative values actually denote IVO and EVC events separation, i.e. the exhaust valve closes before the intake valve opens) to +42 CA degrees. The diluent fraction, determined by sampling the cylinder charge during the compression stroke as explained in section 2.4, varied in the range 6 to 26% of the total trapped mass. An inter-cooled external EGR system was also fitted to the test engine to gain a certain degree of control over the charge dilution level, independently of the valve timing setting. The same system allowed running separate experiments where the changes brought about by the temperature of the recycled gases were observed.

http://dx.doi.org/10.5772/55495

Variable	Units	Values/Description
Test-engine configuration	-	In-line four-cylinder
Bore	mm	79.0
Stroke	mm	81.4
Ratio of con-rod to crank radius	-	3.37
Compression ratio	-	11
Swept volume/cylinder	cm^3	399
Number of valves/cylinder	-	4
Intake valves diameter	mm	27.6
Exhaust valves diameter	mm	21.4
Intake valves maximum lift	mm	7.3
Exhaust valves maximum lift	mm	6.98
Engine Layout	-	Double Over-Head Camshaft
Maximum power	kW	74 @ 6000 rev/min
Maximum torque	Nm	145 @ 4000 rev/min
Fuel injection system	-	Sequential multi-point

Table 1. Specifications of the test engine.

A piezo-electric pressure transducer was installed flush-mounted in one cylinder to acquire in-cylinder pressure variation with 1 CA degree resolution. Ensemble-averaged values of pressure, calculated over batches of 100 consecutive cycles, were used to evaluate the MFB characteristics with the Rassweiler and Withrow methodology. The application details and limitations associated to this have been discussed in section 3.1. Values of combustion duration (in particular, FDA and RBA) were extracted from these and correlated with the relevant operating variables. The following sub-section explores how combustion duration varies as a result of changes to the valve overlap interval. An investigation on the influence of engine operating variables, varied in isolation at fixed valve timing setting, is also presented.

4.2. Influence of valve timing on combustion duration

The influence of the valve timing strategy on dilution mass fraction and on the duration of combustion is presented here. As discussed in section 2.3.2, valve timing exerts a strong influence on mixture preparation by altering the amount of exhaust gas internally recirculated from one engine cycle to the following one. Dilution mass fraction measurements as a function of valve overlap are presented in figures 3 and 4 for three representative engine speeds, at each of two fixed engine loads (kept constant by acting on the throttle valve position) and spark timings. The spark ignition advance was kept unvaried at 25 CA degrees BTDC for the low load cases and at 14 CA degrees BTDC for the high load cases. The valve timing setting was

changed as described in section 4.1; figure 3 refers to fixed EVC timing and figure 4, which shows similar distributions, refers to fixed IVO timing. Levels of dilution are greatest at low-load, low-speed conditions, because of a stronger exhaust gas back-flow when the intake and exhaust valves are overlapping. As expected, dilution mass fraction is an increasing function of valve overlap and, across regions of positive overlaps, it rises at increasing rate as the overlap value increases. For small values of either positive or negative valve overlap, the dilution fraction is relatively constant. When the valve overlap grows negatively (producing wider valve events separation), relatively small increments in dilution are due to early EVC, which has the effect of trapping more residuals, or to late IVO, which reduces the amount of fresh air trapped inside the cylinder.

Representative results for the 0 to 10% MFB duration (FDA) are given in figures 5 and 6; those for the 10 to 90% MFB duration (RBA) are given in figures 7 and 8. The burn angles are plotted for three engine speeds and two levels of IMEP and spark advance. Both FDA and RBA increase consistently with increasing values of positive valve overlap. The increase in RBA is more pronounced than that in FDA, and proportionately greatest at low-load conditions (2.5 bar IMEP). The variations with overlap are similar for fixed intake and fixed exhaust timings, indicating that overlap phasing about TDC is not critical and the influence on combustion is exerted primarily through the overlap extension. The plotted trends are similar at all three engine speeds considered, with a small offset which reflects the inherent increase in burn duration as the speed increases. For small positive overlaps and for negative overlaps the burn angles do not show evident correlation with valve overlap. In these regions, the back-flow into the cylinder is reduced or does not occur at all, indicating that dilution mass fraction is the main cause of combustion duration alterations. Figure 5 to 8 show data which refer to operating conditions at which some variations of combustion duration was actually found. For running conditions exceeding about 6 bar IMEP and 3000 rev/min, combustion duration is almost independent of the valve timing setting.

The analysis of figures 3 to 8 suggests that the influence of dilution accounts for most of the variation in the rate of combustion with variable valve overlap. The effect of valve timing exerted through modifications to bulk motion and turbulence was not apparent in the data. Plots of RBA against dilution (not included here, but available in [42]) depict linear trends with gradients of variation only slightly biased towards greater engine speeds, and also independent of the valve overlap phasing. Similar conclusions for part-load running conditions and intake valve-only variations have been drawn by Bozza et al. in [43], whereas Sandquist et al. [44] observed that the linearity between burn angles and charge dilution held only for fixed phasing, indicating that a dependence upon engine design is possible. The FDA also increases linearly with dilution mass fraction, though at a much weaker rate.

4.3. Influence of other operating variables on combustion duration

The influence of charge dilution upon rate and duration of combustion was explored also by means of separate tests carried out at fixed valve timing setting, to minimize any potential underlying influence on combustion, and using variable amounts of external EGR. Valve timing was set at default configuration, i.e. IVO = +6 CA degrees BTDC, and EVC = +6 CA

http://dx.doi.org/10.5772/55495

degrees ATDC. Figure 9 illustrates the general effect of increasing charge dilution on MFB and burning rate characteristics, for fixed engine speed of 1900 rev/min and fixed intake pressure of 60 kPa. As expected, increasing dilution tends to reduce the strength of combustion, as indicated by the peak burning rate in kg/s, and stretches its duration over larger CA intervals for both the development and the rapid burning stages. Representative results for the variation of FDA and RBA with dilution mass fraction for three engines speed, at each of two engine loads and spark advances, are given in figures 10 and 11. Both combustion intervals are seen to increase linearly at a rate which is essentially independent of engine load and spark timing [45]. As discussed in the previous section, the gradients of these linear correlations, particularly for the RBA, are only slightly biased towards greater engine speeds, as a result of extending combustion further along the expansion stroke, into regions of lower temperature and pressure. When the level of dilution is varied by means of cooled external-EGR, combustion duration increases at a slightly higher rate than the case of dilution changes from increasing valve overlap. This is explained considering that charge temperature and charge density variations, which occur at the same time as dilution changes when the valve timing is modified, tend to moderate the influence of dilution on burn rate.

Figures 12 to 14 illustrate the effects of engine speed, load and spark advance on combustion duration. Experimental data were again recorded under default valve timing setting, and the dilution level was kept unvaried by using appropriate rates of external EGR. In figure 12, the FDA and the RBA increase almost linearly with increasing engine speed, with gradients of variation which appear independent of engine load. The RBA increases more rapidly than the FDA because, as discussed above, greater engine speed would stretch the rapid stage of combustion further into the expansion stroke. Engine speed, as discussed in section 2.2, is directly proportional to turbulence intensity and therefore greater engine speed would lead to an augmented rate of combustion by means of increased unburned gas entrainment into the propagating flame front. However, increasing speed extends the burn process over wider CA intervals and the effect of greater turbulence intensity is only to moderate such extension. Doubling the engine speed between 1500 rev/min and 3000 rev/min stretches FDA by about 1/3 and RBA by 1/2. Figure 13 shows that FDA and RBA decrease linearly when plotted as a function of engine load, in terms of IMEP, at constant level of dilution mass fraction. Both burn angles decrease linearly also with increasing intake manifold pressure. The RBA decreases at an average rate of 2.7 CA degrees per 10 kPa increase in intake manifold pressure. The FDA decreases at a rate which is approximately half of the one calculated for the RBA. Some representative results concerning the variation of the burn angles with the degree of ST advance, at fixed dilution, are illustrated in figure 14. As the ignition timing is advanced towards the MBT setting, combustion initiates earlier in the compression stroke, i.e. at lower temperatures and pressures. Under the influence of these less favourable conditions for flame development, the FDA increases slightly. At the same time RBA, which cover the bulk of combustion duration, tends to decrease as the overall combustion phasing improves. The trends in figure 14 extend to STs more advanced than the MBT values, but the degree of over-advance was limited to 3–4 CA degrees to avoid the inception of knock and this was too small to establish any turning point.

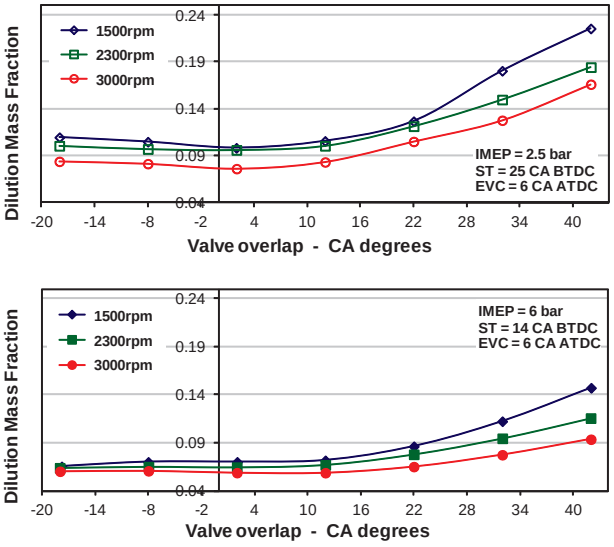

Figure 3. Measured charge dilution mass fraction as function of valve overlap, at constant EVC setting; top plot: light engine load; bottom plot: medium/high engine load.

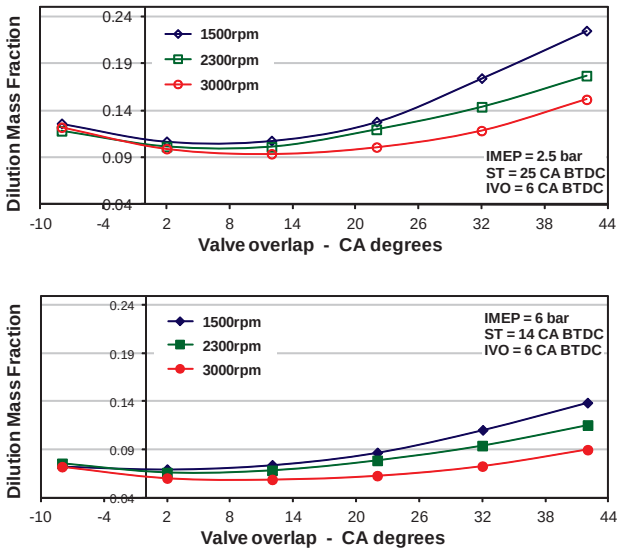

Figure 4. Measured charge dilution mass fraction as function of valve overlap, at constant IVO setting; top plot: light engine load; bottom plot: medium/high engine load.

http://dx.doi.org/10.5772/55495

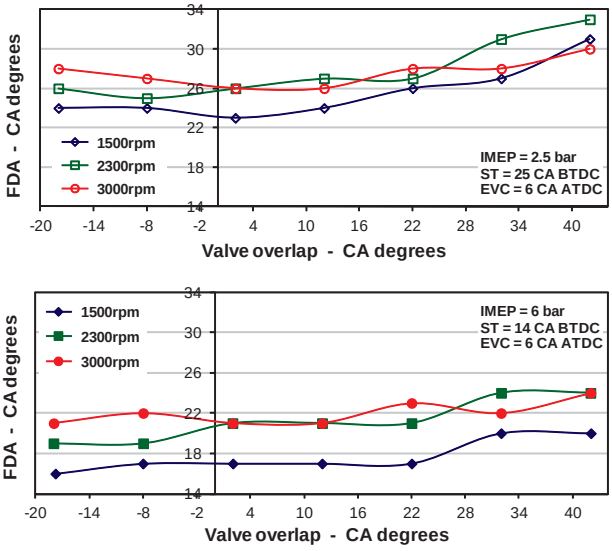

Figure 5. FDA as a function of valve overlap, at constant EVC timing; top plot: light engine load; bottom plot: medium/high engine load.

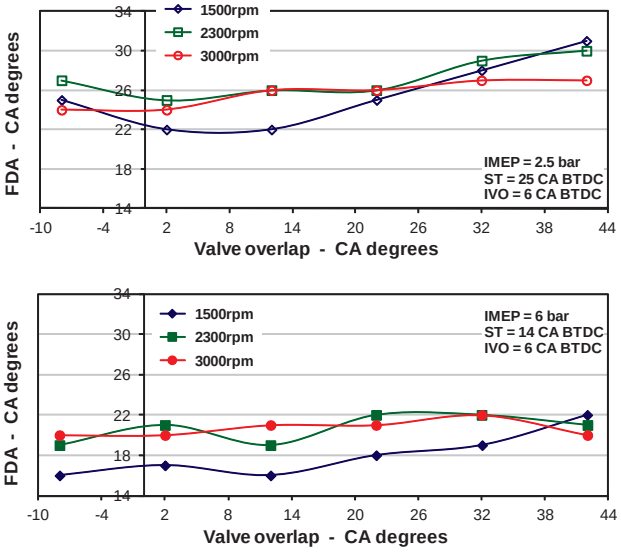

Figure 6. FDA as a function of valve overlap, at constant IVO timing; top plot: light engine load; bottom plot: medium/high engine load

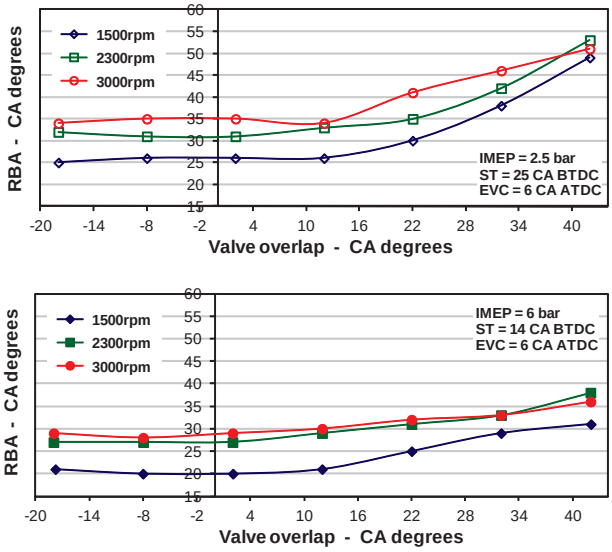

Figure 7. RBA as a function of valve overlap, at constant EVC timing; top plot: light engine load; bottom plot: medium/high engine load.

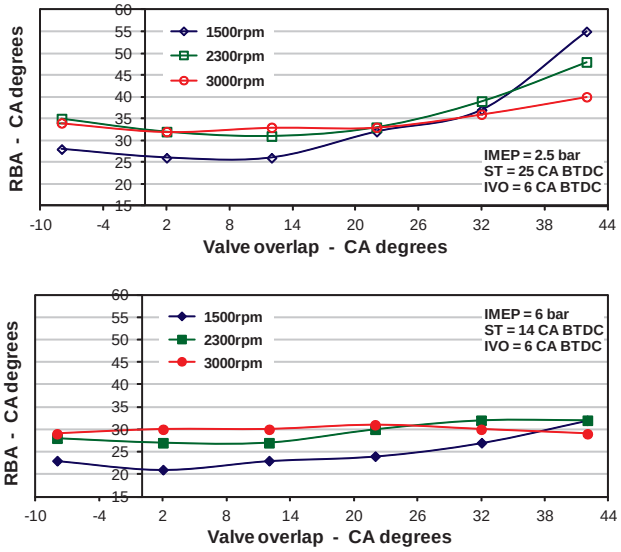

Figure 8. RBA as a function of valve overlap, at constant IVO timing; top plot: light engine load; bottom plot: medium/high engine load.

http://dx.doi.org/10.5772/55495

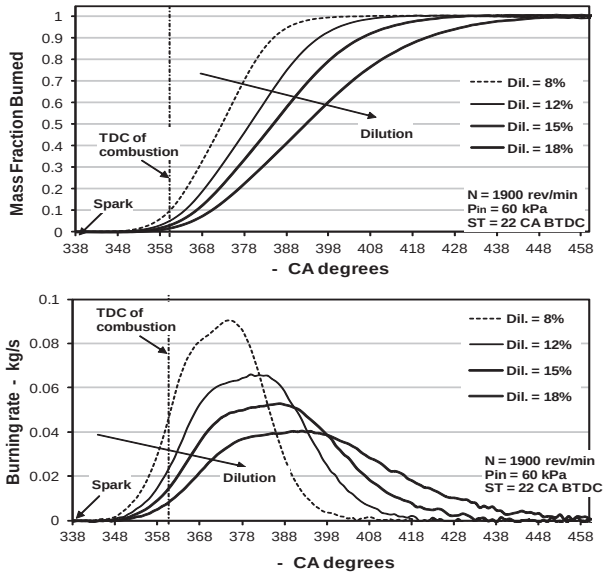

Figure 9. Charge burn characteristics at increasing dilution (by external EGR), for fixed operating conditions (N = 1900 rev/min; Pin = 60 kPa, intake manifold pressure; ST = 22 CA° BTDC) and fixed valve timing setting

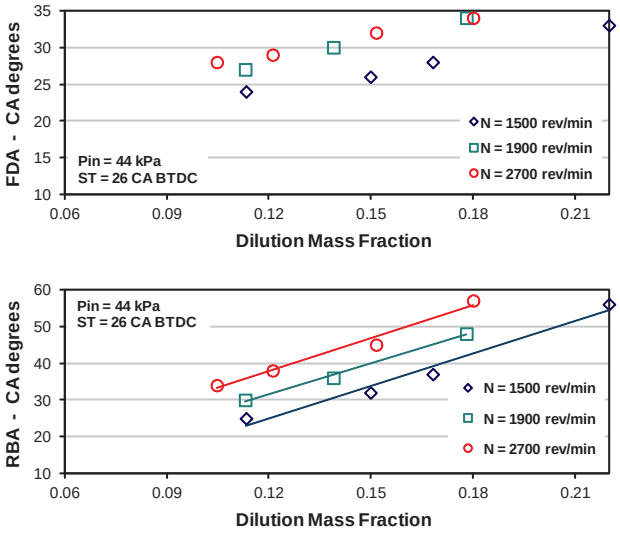

Figure 10. Influence of charge dilution (by external EGR) on burn angle, at low engine load and fixed valve timing.

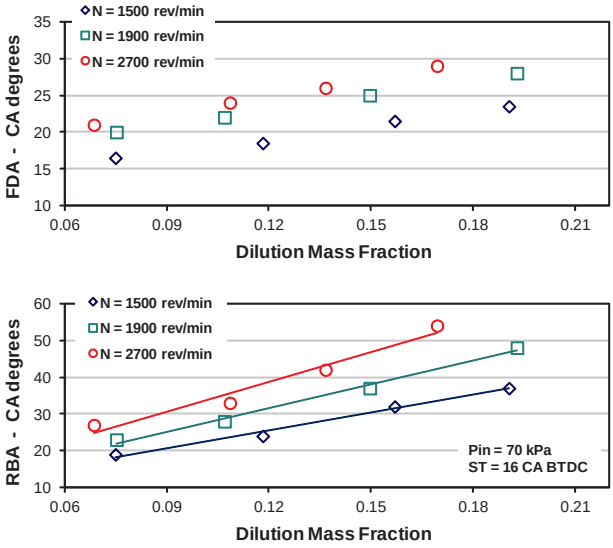

Figure 11. Influence of charge dilution (by external EGR) on burn angles, at medium/high engine load and fixed valve timing

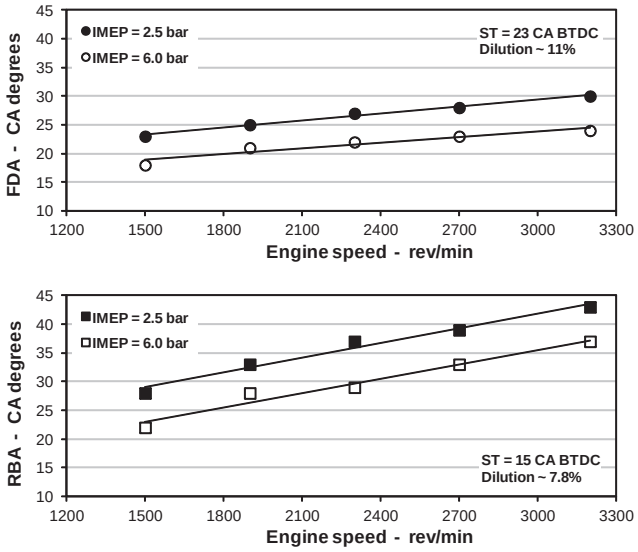

Figure 12. Influence of engine speed on burn angles, at constant level of dilution and fixed valve timing

http://dx.doi.org/10.5772/55495

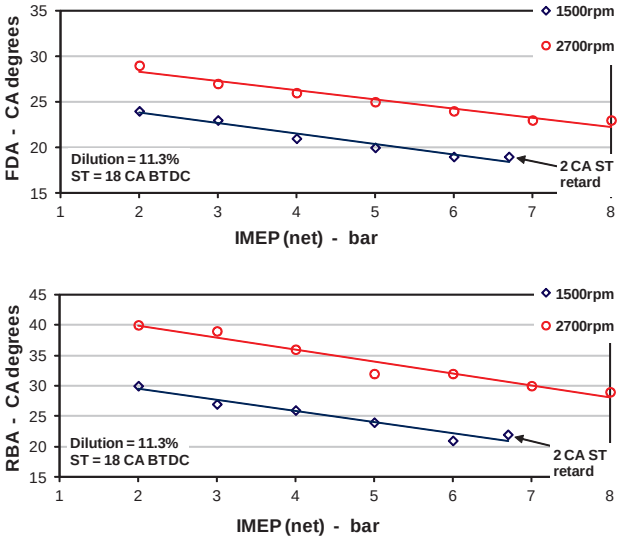

Figure 13. Influence of engine load on burn angles, at constant level of dilution, and fixed valve timing.

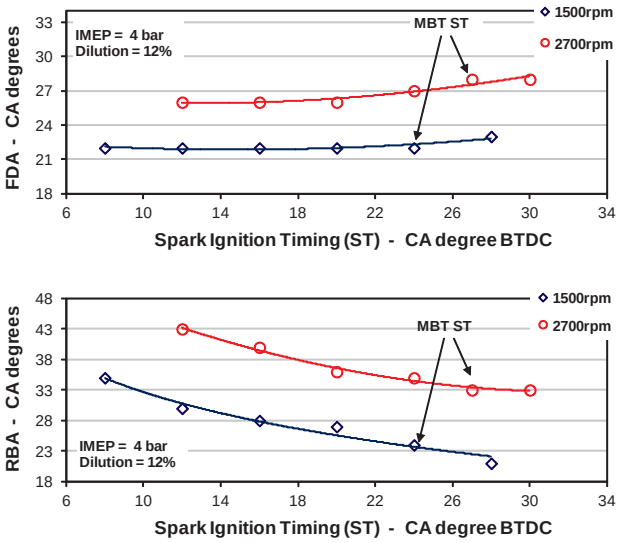

Figure 14. Influence of spark timing advance on burn angles, at constant level of dilution and fixed valve timing.

5. Simplified combustion modelling

The ability to describe analytically the charge burn process in SI engines, capturing the details of the most relevant influences on this, is essential for both diagnosis of performance and control requirements. The empirical combustion models that enable just the above ability are usually called non-dimensional or zero-dimensional models, because they do not incorporate any explicit reference to combustion chamber geometry and flame front propagation. Such approaches typically output the burn rate or the MFB profile in the CA domain and require several stages of calibration by fitting real engine data to appropriate analytical functions. One of the most widely used methods in engines research is to carry out curve fits of experimental MFB curves to describe the combustion evolution via a Wiebe Function,

$$x_{MFB}\left(\vartheta\right) = 1 - EXP\left[-a\left(\frac{\vartheta - \vartheta_{ST}}{\Delta\vartheta}\right)^{n}\right] \tag{20}$$

where ϑ is the generic CA location, ϑ_{ST} is the CA location of combustion initiation, $\Delta\vartheta$ is the total combustion angle, a and n are adjustable parameters called efficiency and form factor. Owing to its simplicity and robustness of implementation the Wiebe function represents a convenient platform for extracting signals from the noises of the sensing elements and lends itself ideally for inclusion into model-based control algorithms. Section 5.1 explores derivation, experience of use and limitations of a Wiebe function-based model of the MFB profile, originally presented by the Author in [46], and developed using experimental data from the same modern-design gasoline engine described in section 4.

A different type of combustion models are the so-called phenomenological or quasi-dimensional models. These require spatial subdivision of the combustion space into zones of different temperature and chemical composition (two zones, burned and unburned, in their simplest version) and are often used to evaluate both combustion of fuel and associated pollutant formation. Phenomenological models are based on more fundamental theoretical principles, hence they should be *transportable* between engines of different size and geometry. Nevertheless, these models also require some form of calibration using real measurements. Recent published work by Hall et al. [47] and by Prucka et al. [5] offers examples of relatively simple phenomenological flame propagation and entrainment models, suited for inclusion into fast-execution ST control algorithms, to ensure optimal phasing of the 50% MFB location (i.e. 7 or 8 CA degree ATDC) and improve engine efficiency and fuel economy. In these models, the instantaneous rate of combustion is calculated fundamentally, through some modifications of the basic equation of mass continuity $dm_b/d\tau = \rho_u A S_b$. Section 5.2 illustrates one of these models, along with results which highlight the influence of relevant engine operating variables on combustion for a modern flexible-fuel engine.

http://dx.doi.org/10.5772/55495

5.1. Combustion modelling using the Wiebe function

One of the most comprehensive accounts of rationale and applications of the Wiebe function as a burn rate model is due to J. I. Ghojel, in his recent *tribute to the lasting legacy of the Wiebe function and to the man behind it, Ivan Ivanovitch Wiebe* [48]. The purpose of the original work by Wiebe was to develop a macroscopic reaction rate expression to bypass the complex chemical kinetics of all the reactions taking place in engine combustion. The result, which is typically based on a law of normal distribution representing the engine burning rate, is a very flexible function, heavily used in the last few decades to model all forms and modes of combustion, including compression and spark ignition, direct and indirect injection and homogeneous charge compression ignition combustion, with a range of liquid and gaseous fuels. An extensive survey on the implementation of the Wiebe function (as well as some mathematical modifications) has been also carried out by Oppenheim et al. [49]. Here the authors recognise the practical virtues of the function and its well-established use, but question its derivation, which is described as a *gigantic leap* from chemical kinetics of the exothermic reactions of combustion to the consumption of fuel.

5.1.1. Methodology

The aim of the investigation is to model the S-shaped MFB profile from combustion initiation (assumed to coincide with spark timing) to termination (100% MFB), using the independent parameters of the Wiebe function. The total burning angle is taken as the 0 to 90% burn interval, $\Delta\vartheta_{90}$, preferred to the 0-99.9% interval used in other work (for example [50]) as the point of 90% MFB can be determined experimentally with greater certainty. Especially for highly-diluted, slow-burning combustion events the termination stage cannot be described accurately from experimental pressure records, as the relatively small amount of heat released from combustion of fuel is comparable to co-existing heat losses, e.g. to the cylinder walls [51]. For these reasons, using the $\Delta\vartheta_{90}$ rather than the $\Delta\vartheta_{99.9}$ as total combustion angle should ascribe increased accuracy to the overall combustion model. It can be demonstrated that, with the above choice of total combustion angle, the efficiency factor a takes a unique value of 2.3026. $\Delta\vartheta_{90}$ and n remain as independent parameters and curve fits to experimental MFB curves allow correlating these to measurable or inferred engine variables.

The experimental data used for model calibration have been collected using the research engine described in section 4.1. All tests were carried out under steady-state, fully-warm operating conditions which covered ranges of engine speed, load, spark advance and cylinder charge dilution typical of urban and cruise driving conditions. Data were recorded using always stoichiometric mixtures. Dilution mass fraction, determined from measurements of molar concentrations of carbon dioxide as indicated in section 2.4, was varied either via an inter-cooled external-EGR system or adjusting the degree of valves overlap via the computerised engine-rig controller. Intake and exhaust valve timing were varied independently to set overlap intervals from -20 to +42 CA degrees. The ranges of engine variables covered in this work are the same as those reported in section 4.1. The experimental database included in excess of 300 test-points. Data collected varying the valve timing setting were kept separately

and used for purposes of model validation. MFB profiles at each test-point were built applying the Rassweiler and Withrow methodology to ensemble-averaged pressure traces. The FDA, 50% MFB duration ($\Delta\vartheta_{50}$) and RBA were calculated from these curves, using a linear interpolation between two successive crank angles across 10%, 50% and 90% MFB to improve the accuracy of the calculations.

The combustion process in premixed gasoline engines is influenced by a wide range of engine specific as well as operating variables. Some of these variables, such as the valve timing setting, can be continuously varied to achieve optimum thermal efficiency (e.g. by improving cylinder filling and reducing pumping losses) or to meet ever more stringent emissions regulations (e.g. by increasing the burned gas fraction to control the nitrogen oxides emissions). There is some consensus in recent SI engine combustion literature upon the variables which are *essential and sufficient* to model the charge burn process in the context of current-design SI engines [23, 45, 50, 52, 53, 54, 55, 56]. For stoichiometric combustion, in decreasing rank of importance these are charge dilution by burned gas, engine speed, ignition timing and charge density. In the present work dilution mass fraction has been of particular interest as large dilution variations produced by both valve timing setting and external-EGR are part of current combustion and emissions control strategies.

5.1.2. Models derivation

Empirical correlations for the two independent parameters of the Wiebe function, the total burn angle, $\Delta\vartheta_{90}$ and the form factor, n , have been developed carrying out least mean square fits of functional expressions of engine variables to combustion duration data. Whenever possible, power law functions were used in order to minimise the need for calibration coefficients. The choice of each term is made to best fit the available experimental data.

The 0 to 90% MFB combustion angle is expressed as the product of 4 functional factors, whose influence is assumed to be independent and separable:

$$\Delta\vartheta_{90} = k\ R\left(\rho_{ST}\right)\ S\left(N\right)\ X\left(x_b\right)\ T\left(\vartheta_{ST}\right) \tag{21}$$

The functions $S(N)$, $X(x_b)$ and $T(\vartheta_{ST})$ are based upon previously proposed expression, which are reviewed, along with their modifications, in Table 2. With the best-fit numerical coefficients from reference [46], the dimensional constant k was determined to be 178 when density ρ_{ST} is in kg/m^3, mean piston speed S_P is in m/s, the dilution mass fraction is dimensionless, and the spark timing ϑ_{ST} is in CA degrees BTDC. For the spark ignition term, $T(\vartheta_{ST})$, a second-order polynomial fit has been preferred to the hyperbolic function ($a + b/\sqrt{\vartheta_{ST}}$) proposed by Csallner [52] and Witt [53] as it is deemed to retain stronger physical meaning, showing a turning point for very advanced spark timing settings. Advancing the spark ignition generally shortens the total burn duration as combustion is phased nearer TDC; it is expected though that excessively low initial pressure and temperature would change this trend, producing

http://dx.doi.org/10.5772/55495

slower combustion (and increasing combustion duration) for overly advanced spark ignition settings (in excess of 35 CA degrees BTDC). The net effect of engine speed (or mean piston speed) on burn duration is accounted for by an hyperbolic term $S(N)$. Turbulence intensity in the vicinity of the spark-plug has been shown to be directly proportional to engine speed (see section 2.2 above); hence increasing engine speed enhances the burning rate via greater combustion chamber turbulence. In truth, in a modern engine there is a number of factors, including intake and exhaust valve timing, which may have an impact on turbulence intensity. Different sources spanning across several decades continue to indicate that the main driver for in-cylinder turbulence is engine speed and that other factors actually exert only a minor influence [12, 20, 21, 46, 47, 57]. However, increasing engine speed also extends the burn process over wider CA intervals and the effect of greater turbulence is only to moderate such extension.

Function	$R(\rho_{ST})$	$S(N)$	$X(x_b)$	$T(\vartheta_{ST})$
Analytical Form	$\left(\frac{1}{\rho_{ST}}\right)^{\beta}$	$a+\frac{b}{\sqrt{S_P}}$	$\left(1-2.06\ x_b^{0.77}\right)^{\gamma}$	$c\ \vartheta_{ST}^2+d\ \vartheta_{ST}+e$
Hires et al. 1978 [23]	-	-	$\left(\frac{1}{1-2.06\ x_b^{0.77}}\right)^{0.67}$	-
Csallner. 1981 [52]	-	$1-\frac{13.65}{\sqrt{N}}$	-	-
Witt. 1999 [53]	-	$1-\frac{13.65}{\sqrt{N}}$	-	-
Bayraktar et al. 2004 [54]	-	-	-	$0.238\left(\frac{\vartheta_{ST}}{\vartheta_1}\right)^2-0.272\frac{\vartheta_{ST}}{\vartheta_1}+1$
Scharrer et al. 2004 [45]	-	$1-\frac{13.65}{\sqrt{N}}$	-	-
Vávra et al. 2004 [55]	-	-	-	$0.233\left(\frac{\vartheta_{ST}}{\vartheta_1}\right)^2-0.664\ \frac{\vartheta_{ST}}{\vartheta_1}+1$
Lindstöm et al. 2005 [50]	-	$1-\frac{1.39}{\sqrt{S_P}}$	$\left(\frac{1}{1-2.06\ x_b^{0.77}}\right)$	$5.69x10^{-4}\ \vartheta_{ST}^2-0.033\ \vartheta_{ST}+1$
Bonatesta et al. 2010 [46]	$\left(\frac{1}{\rho_{ST}}\right)^{0.34}$	$1-\frac{1.164}{\sqrt{S_P}}$	$\left(\frac{1}{1-2.06\ x_b^{0.77}}\right)^{0.85}$	$0.00033\ \vartheta_{ST}^2-0.0263\ \vartheta_{ST}+1$
Galindo et al. 2011 [56]	$\left(\frac{1}{\rho_{ST}}\right)^{0.34}$	$1-\frac{0.8}{\sqrt{S_P}}$	$\left(\frac{1}{1-2.06\ x_b^{0.46}}\right)^{0.85}$	$0.0004\ \vartheta_{ST}^2-0.024\ \vartheta_{ST}+1$

Table 2. Functional expressions used in [46] to account for the influence of operating variables on the total burn angle, along with similar published expressions.

The influence of charge dilution by burned gas on combustion duration is accounted for via a power law of the function $(1-2.06x_b^{0.77})$, originally identified by Rhodes and Keck [58] and by Metghalchi and Keck [59] to represent the detrimental influence of burned gas on the laminar burning velocity. The power correlation given by $X(x_b)$ was retrieved changing the dilution fraction over the range 6 to 26% via external-EGR (with fixed, default valve timing setting), to minimise the disturbing influence of valve timing on other factors such as cylinder filling. Figure 15 illustrates how the density function, $R(\rho_{ST})$, with power index set to 0.34, fits to data recorded over a range of engine loads between 2 and 7 bar net IMEP, at each of three engine speeds. During these load sweeps, the spark timing and level of dilution, which would normally change with load as a result of changing exhaust to intake pressure differential, were set constant.

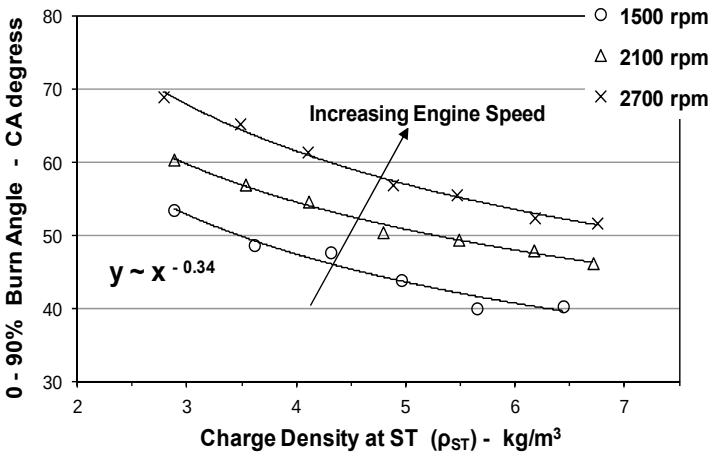

Figure 15. Total burning angle as a function of charge density at constant spark timing and constant dilution mass fraction for three engine speeds. Adapted from reference [46].

The density function was introduced in [46] to account for a further observed influence of engine load on combustion duration, not fully captured by the empirical terms developed for the dilution fraction or the spark ignition setting. The same density expression has been adopted more recently by Galindo et al. [56] in a work devoted to modelling the charge burn curve in small, high-speed, two-stroke, gasoline engines using a Wiebe function-based approach.

The final correlation developed for the total 0 to 90% MFB burning duration is written as:

$$\Delta\vartheta_{90} = 178\left(\frac{1}{\rho_{ST}}\right)^{0.34}\left(1-\frac{1.164}{\sqrt{S_P}}\right)\left(\frac{1}{1-2.06\ x_b^{0.77}}\right)^{0.85}\left(0.00033\ \vartheta_{ST}^2 - 0.0263\ \vartheta_{ST} + 1\right) \qquad (22)$$

http://dx.doi.org/10.5772/55495

Its accuracy was tested across the whole 300-point-wide experimental database, featuring combinations of engine variables limited by the ranges discussed in section 4.1. Part of this database, including the VVT data, was used for model validation only. Values of $\Delta\vartheta_{90}$ generated using equation (22) showed a maximum prediction error of 11%, while three-quarters of the data fell within the ±5% error bands.

Values of form factor n used to build the second empirical correlation advanced in [46], have been determined by minimising the error of the least square fit to the MFB profile. A covariance regression model with a weighting power function (weight factor α),

$$\frac{1}{N}\sum \frac{\left(MFB_{Wiebe} - MFB_{\exp}\right)^2}{\left(MFB_{\exp}\right)^{\alpha}} \tag{23}$$

was minimised to achieve a balanced fit across the burn profile from the start of combustion and up to the 50% MFB location. As evident from the error analysis illustrated in figure 16, as the weight factor α increases the absolute fitting error in FDA falls, whereas the one in $\Delta\vartheta_{50}$ tends to increase at least for durations in excess of 40 CA degrees. A weight factor of 0.3 allows limiting the error in both FDA and $\Delta\vartheta_{50}$ to within 5%, but other strategies can be followed depending on the ultimate target of the combustion modelling exercise.

Using the values of n determined as described above, the form factor has been related to the product of functions of mean piston speed, spark timing and charge dilution mass fraction, as follows:

$$n = 3.46 \left(\frac{1}{\sqrt{S_P}}\right)^{0.45} \left(\frac{1}{1+\sqrt{\vartheta_{ST}}}\right)^{-0.35} \left(1 - 1.28\ x_b\right) \tag{24}$$

In this expression the mean piston speed S_P is in m/s, the dilution mass fraction is dimensionless, and the spark timing ϑ_{ST} is in CA degrees BTDC. The choice of functional expressions of relevant engine parameters has no physical basis beyond best-fitting trends to the selected experimental data. The influence of charge density on combustion evolution was not evident in the results for the Wiebe function form factor. The values of form factor generated using equation (24) were within ±8% of those deduced from individual MFB curves for the whole range of experimental conditions used for model validation, including the data recorded with variable valve timing setting. Similar functions of the same engine variables have been developed by Galindo et al. [56], using combustion records from two high-speed 2-stroke engines, strengthening to some extent the validity of the form factor modelling approach.

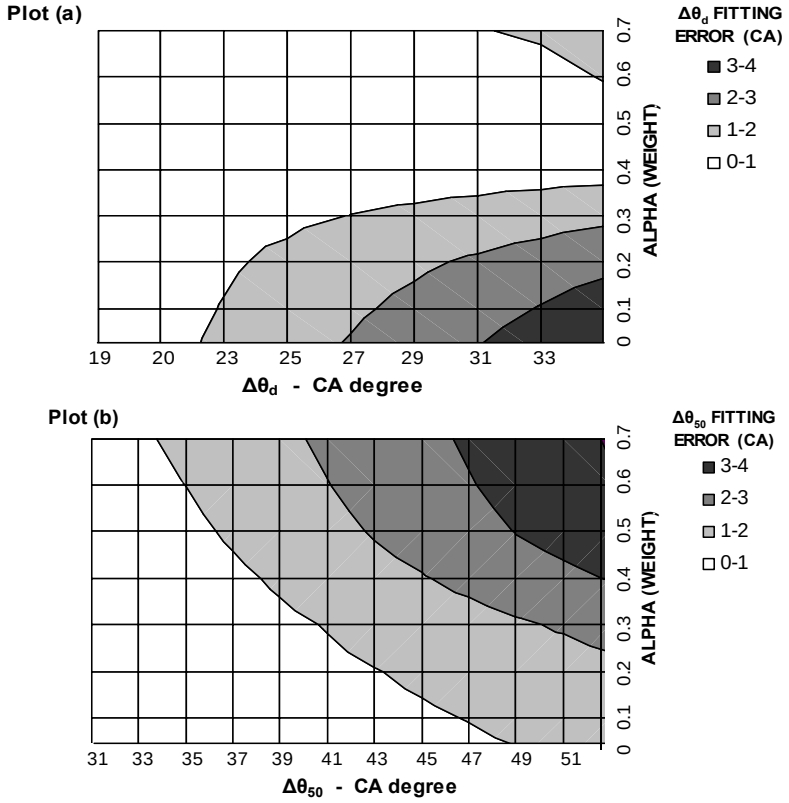

Figure 16. Plot (a): Wiebe function fitting error in FDA ($\Delta\vartheta_d$) for different weighting factors; Plot (b): Wiebe function fitting error in $\Delta\vartheta_{50}$ for different weighting factors. Adapted from reference [46].

5.1.3. Discussion of results and accuracy

Expressions for the 0-90% MFB angle and the form factor of the Wiebe function have been derived empirically to represent the burn rate characteristics of a modern-design SI engine featuring VVT. Four factors – dilution mass fraction, engine speed, ignition timing and charge density at ignition location, were used to describe the evolution of premixed SI gasoline combustion. The range of engine operating conditions examined covered a large portion of the part-load envelope and high levels of dilution by burned gas. Valve timing influences combustion duration mostly through changes in the levels of dilution and in-cylinder filling; the results show that these influences are captured by the proposed models. Other effects which might results from valve timing changes, such as the changes in turbulence level, appear to be secondary and no explicit account of these has been required [46, 47, 60].

Average errors in FDA, RBA and $\Delta\vartheta_{50}$, calculated using the Wiebe function with modelled inputs, were in the region of 4.5%; maximum errors across the whole database were within the

http://dx.doi.org/10.5772/55495

13% error bands. This magnitude of uncertainty is typical of simplified thermodynamics combustion models applied to engines with flexible controls. Importantly, the analysis has shown that errors of magnitude up to 7% would be expected due to the inherent limitations of fitting a Wiebe function to an experimental MFB profile [46]. Further error analysis shows that the expected errors in the various combustion duration indicators are proportional to those in $\Delta\vartheta_{90}$. Overestimates of the form factor increase the predicted FDA and reduce the RBA. The influence of n upon $\Delta\vartheta_{50}$ is instead relatively small; this suggests the approach presented here may be applicable to combustion phasing control.

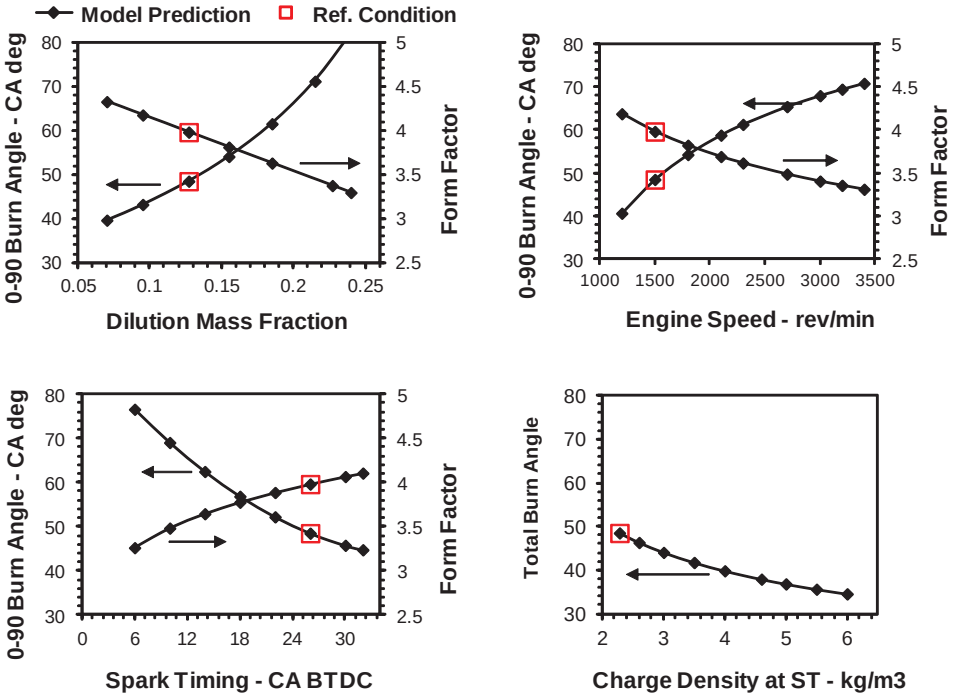

Figure 17. Parametric variation of $\Delta\vartheta_{90}$ and form factor from given baseline conditions: N = 1500 rev/min, Pin = 45 kPa (corresponding to spark timing density of 2.3 kg/m^3), Dilution Mass Fraction = 12.7%. Adapted from reference [46].

The sensitivities of the 0-90% MFB burn angle ($\Delta\vartheta_{90}$) and form factor to changes in the chosen relevant engine parameters, using a typical part-load operating condition as a baseline, are shown in figure 17. The influence of increasing charge density is least significant, producing the smallest reductions in burn duration. This does not fully account for the effect of changes in engine load, which would usually produce changes in dilution level as well as charge density. Increasing engine speed or the level of dilution produces an increase in the burn angle and a reduction in the form factor. Spark timing advances show opposite effects. The average

changes in $\Delta\vartheta_{90}$ are of the order of one CA degree per half per cent increase in dilution or 80 rev/min increase in engine speed. The sensitivity of form factor to engine speed and level of dilution is similar to that reported in [50].

The wider applicability of the proposed equations was also tested by comparing predictions with experimental combustion duration data reported in [50] for a turbocharged SI engine of similar design (see figure 18). Importantly, the comparison was made for intake manifold pressures above 1 bar, i.e. above the load range used for model derivation. The results show that the offset between experimental and modelled combustion angles is virtually eliminated when the dilution mass fraction of the reference (baseline) conditions is assumed to be 7%, suggesting a value of only 3% as given in [50] may actually be an underestimate.

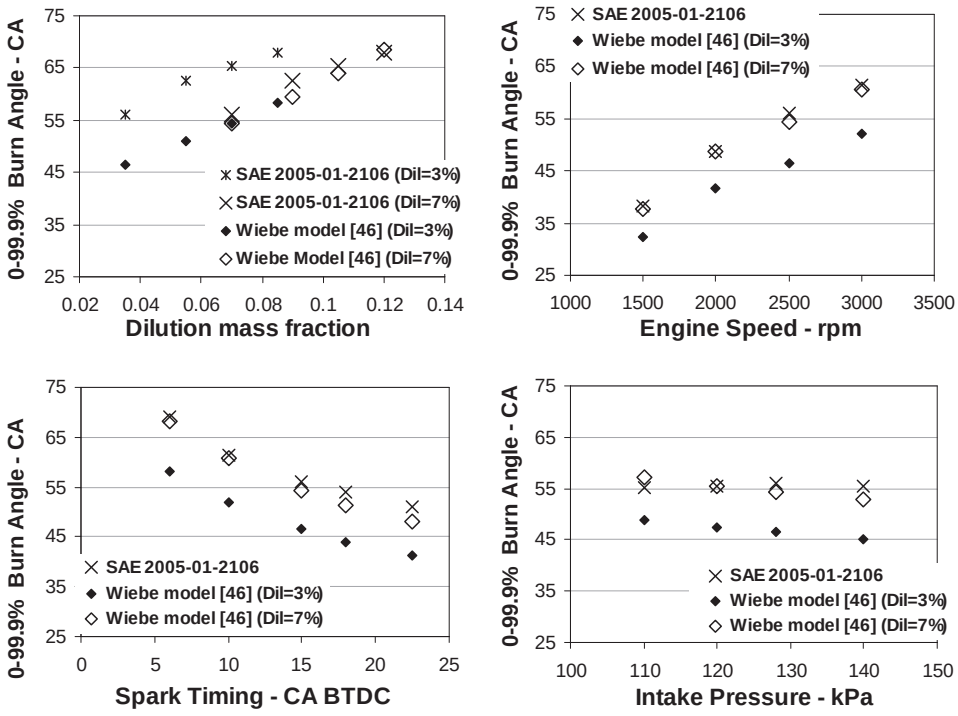

Figure 18. 0 to 99.9% MFB burn angle model predictions compared to published data from SAE 2005-01-2106. Adapted from reference [46].

5.2. Flame propagation modelling

As discussed previously, locating the 50% MFB event at 7 or 8 CA past TDC has been correlated to achieving best fuel efficiency in SI engine combustion. The recent work by Hall et al. [47] outlines a relatively simple, physics-based, quasi-dimensional flame propagation model capable

http://dx.doi.org/10.5772/55495

of capturing the influence of variable valve timing, ethanol/gasoline blend ratio and other parameters relevant to modern SI engines, to provide estimates of the 50% MFB location and hence phase the combustion period most appropriately with respect to TDC. The model advanced by Prucka et al. [5] is similarly used for predicting best ignition timing in complex SI engine architectures (featuring not only VVT technology but also a charge motion control valve), but it is different in its logic as it relies on a simplified adaptation of the turbulent flame entrainment concept originally introduced by Blizard and Keck [61]. The present section introduces the reader to the first type of combustion models, which is less reliant on complex descriptions of fuel burning rate and turbulence regimes, and hence more readily implementable.

5.2.1. Assumptions and methodology

Simplified flame propagation models tend to use readily available measurements from sensors and output estimates of ignition timing to achieve best efficiency for given engine running conditions. The basic inputs can be listed as follows:

- engine speed
- mass of fuel injected and ethanol/gasoline ratio
- equivalent ratio (or air-to-fuel ratio)
- spark timing and relative thermodynamic conditions (temperature, pressure and charge density)
- dilution mass fraction or charge characterization (masses of fresh air and burned gas trapped at IVC)

Charge dilution should be measured or estimated through gas exchange modelling, exploiting values for intake and exhaust manifold pressure as well as available cylinder volume at the IVO and at the EVC event. The exhaust manifold temperature appears in the calculations, weakening (due to the inherent slow response time of temperature sensors) the applicability of the approach to transient operation. In Hall et al. [47] the degree of positive valve overlap is considered directly responsible for the charge characterization, while modulation of valve lift and, more in general, changes of valve opening profiles, which may directly affect the level of turbulence, are not investigated.

The in-cylinder thermodynamic conditions at the time of ignition (ST) can be calculated assuming polytropic compression from IVC conditions:

$$P_{ST} = P_{IVC}\left(V_{IVC} / V_{ST}\right)^{n} \tag{25}$$

$$T_{ST} = T_{IVC}\left(V_{IVC} / V_{ST}\right)^{n-1} \tag{26}$$

In-cylinder pressure at IVC can be assumed to be approximately equal to the intake manifold pressure; charge temperature at IVC can be expressed as the weighted average of fresh air temperature (intake temperature, T_{in}) and hot, recirculated gas temperature (exhaust temperature, T_{ex}):

$$T_{IVC} = x_b \; T_{ex} + \left(1 - x_b\right) \; T_{in} \tag{27}$$

The polytropic index of compression n does vary with engine conditions, but a constant value of 1.29 has been used to yield acceptable overall results [47]; some researchers [5] have suggested a linear fit to measured or estimated values of charge dilution mass fraction. The charge density at spark timing is calculated from pressure and temperature advancing the hypothesis of ideal gas mixture, or simply by the ratio of total trapped mass m_{tot} and available chamber volume V_{ST} .

Following spark ignition, the combustion process commences and a thin quasi-spherical flame front develops, separating burned and unburned zones within the combustion chamber. These two regions are supposed to be constantly in a state of pressure equilibrium. The rate of burning, i.e. the rate of formation of burning products (units of kg/s), is calculated step-by-step through the application of the equation of mass continuity (1), repeated here for completeness:

$$\frac{dm_b}{d\tau} = \rho_u \; A \; S_b \tag{28}$$

In this expression ρ_u (units of kg/m^3) is the density of the gas mixture within the unburned zone, A (m^2) can be considered as a mean flame surface area and S_b (m/s) is the turbulent burning velocity. This velocity, in the context of simplified flame propagation models, is loosely assumed to coincide with the turbulent flame velocity. The rate of fuel consumption (rate of change of the mass of fuel burned, m_{fb}) is linked to the above rate of burning through the definition of the air-to-fuel ratio (A/F), which is assumed to be invariable in time (i.e. during the combustion process) and in space (i.e. homogeneous mixture throughout the unburned zone):

$$\frac{dm_{fb}}{d\tau} = \left(A/F\right)^{-1} \; \frac{dm_b}{d\tau} \tag{29}$$

Equation (28) can be rewritten to define the rate of change of mass fraction burned (here indicated as x_{MFB}) in the time domain:

http://dx.doi.org/10.5772/55495

$$\frac{dx_{MFB}}{d\tau} = \frac{1}{m_{fc}} \frac{dm_b}{d\tau} = \frac{1}{m_{fc}} \rho_u A S_b \tag{30}$$

In the latter expression, m_{fc} (units of kg) should be the mass of fresh charge, which includes fresh air and fuel only, and not the total trapped mass, which include an incombustible part. If the rate from equation (30) is evaluated in the CA domain, and then integrated over the combustion period, it yields the MFB profile which can be used to identify the location at which 50% of the charge has burned, or other relevant combustion intervals. The conversion of the above rates from the time to the CA domain is carried out observing that time intervals (in seconds) and CA intervals are correlated as $d\vartheta = 6N\, d\tau$, where N is engine speed in rev/min.

The net heat addition rate (units of J/s) due to combustion of fuel can be expressed as:

$$\frac{dQ_{net}}{d\tau} = Q_{LHV} \left[\frac{dm_{fb}}{d\tau} \right] = Q_{LHV} \left[\left(A/F \right)^{-1} m_{fc} \frac{dx_{MFB}}{d\tau} \right] \tag{31}$$

where Q_{LHV} (J/kg) is the lower heating value of the fuel, calculated as a weighted average in case of multi-component fuel blend. Finally, the application of the First Law of the Thermodynamics with the due assumption of ideal gas mixture yields:

$$\frac{dP}{d\tau} = \frac{\gamma - 1}{V} Q_{LHV} \left[\left(A/F \right)^{-1} m_{fc} \frac{dx_{MFB}}{d\tau} \right] - \frac{\gamma P}{V} \frac{dV}{d\tau} \tag{32}$$

used to model the in-cylinder pressure evolution from spark ignition to combustion termination. Within the hypothesis of ideal gas, the ratio of specific heats, γ , should be taken as a constant and given a reasonable average value (for example 1.35). A more realistic approach considers γ as a function of both composition and temperature, quantities which vary and need to be evaluated at each step of the combustion process. Temperature dependent polynomial expressions from the JANAF Thermo-chemical Tables may be used.

5.2.2. Evaluation of burning rate inputs

Commonly [62], the unburned gas density ρ_u needed in equation (28) is estimated by assuming that the unburned charge undergoes a polytropic compression process of given index n from ST conditions due to the expanding flame front:

$$\rho_u = \rho_{ST} \left(P / P_{ST} \right)^{\frac{1}{n}} \tag{33}$$

The pressure input P in this equation would be the value calculated through the application of the First Law, as shown above. Again, a constant value of polytropic compression index can be used to simplify the calculations. The temperature in the unburned region is calculated assuming polytropic compression in a similar fashion. The influence of heat transfer on T_u and hence on the laminar flame speed would be (for simplicity) captured by the empirical tuning factors used within the turbulent flame speed model [47].

One of the major difficulties in modelling SI engine combustion is associated with the identification or the theoretical definition of a burning front or flame surface [22]. In [47] A is a mean flame surface, assumed as such to be infinitely thin and modelled as a sphere during the development stage of combustion. The volume of the burned gas sphere is calculated as the difference between total available chamber volume and unburned gas volume:

$$A = 4\ \pi\ \left(r_{flame}\right)^2\ = 4\ \pi\ \left(\sqrt[3]{3\ V_b / 4\ \pi}\right)^2 = 4\ \pi\ \left(\sqrt[3]{3\ \left(V_{chamber} -\ V_u\right) / 4\ \pi}\right)^2 \tag{34}$$

Some time into the combustion process, the flame front will start impinging cylinder head and piston crown, progressively assuming a quasi-cylindrical shape. After a transition period, the mean flame surface can be modeled as a cylinder whose height is given by the mean combustion chamber height (clearance height) Δh :

$$A = 2\ \pi\ \left(r_{flame}\right)\ \Delta h = 2\ \pi\ \left(\sqrt{V_b / \pi\ \Delta h}\right)\ \Delta h = 2\ \pi\ \left(\sqrt{\left(V_{chamber} -\ V_u\right) / \pi\ \Delta h}\right)\ \Delta h \tag{35}$$

Similar approaches are found in more established literature, dating back to the late 1970s. Referring to a disk-shaped combustion chamber, Hires et al. [23] advance a simple, yet effective, hypothesis of proportionality between *equivalent planar burning surface* and clearance height: $A \propto B\Delta h$, with B the cylinder bore. Of course, the identification of a mean flame surface becomes more challenging in the context of modern combustion chamber geometries such as pent-roof shape chambers; nevertheless, the basic concepts to be adopted in the context of simplified quasi-dimensional combustion modelling remain valid. The topic of SI combustion propagating front, where a fundamental distinction is made between cold sheet-like front, burning surface and thick turbulent brush-like front, is complex and outside the scope of the present work; the interested reader is referred to some established, specialised literature [8, 11, 12, 13, 63].

The turbulent burning or flame speed, S_b , embodies the dependence of the burning rate on turbulence as well as on the thermo-chemical state of the cylinder charge. In time, these dependences have been given various mathematical forms, though all indicate that in-cylinder turbulence acts as an enhancing factor on the leading, laminar-like flame regime. The first turbulent flame propagation model was advanced in 1940 by Damköhler for the so-called wrinkled laminar flame regime [64]. The turbulence burning velocity was expressed as: $S_b = u' + S_L$, where u' is the turbulence intensity and S_L is the laminar burning velocity. An

http://dx.doi.org/10.5772/55495

improvement on this model was proposed by Keck and co-workers [9, 11], showing that during the rapid, quasi-steady combustion phase the turbulent burning velocity assumes the form: $S_b \approx a\, u_T + S_L$, where u_T is a characteristic velocity due to turbulent convection, proportional to unburned gas density as well as mean inlet gas speed. In 1977 Tabaczynski and co-workers developed a detailed description of the turbulent eddy burn-up process to define a semi-fundamental model of the turbulent burning velocity [24].

In [47] the turbulent flame velocity is given as the product of laminar velocity and a turbulence-enhancement factor. In line with the speed/turbulence association discussed above, this factor is expressed as a linear function of engine speed only [57, 65]:

$$S_b = f\, S_L = \left(a\, N + b\right)\, S_L \tag{36}$$

In equation (36) a and b are tuning factors which should be calibrated on each specific engine (their value is 0.0025 and 3.4, respectively, in [47]).

The laminar flame velocity is a quantity which accounts for the thermo-chemical state of the combustible mixture moving into the burning zone. The most classical correlations for laminar velocity have been developed, as mentioned in section 5.1.2, by Rhodes and Keck [58] and Metghalchi and Keck [59]. They used similar power-function expressions to correlate unburned gas temperature, pressure and mixture diluent fraction with laminar velocities measured in spherical, centrally-ignited, high-pressure combustion vessels using multi-component hydrocarbons and alcohols similar to automotive fuels:

$$S_L = S_{L,0} \left(\frac{T_u}{T_{ref}}\right)^{\alpha} \left(\frac{P}{P_{ref}}\right)^{\beta} \left(1 - 2.06\; x_b^{0.77}\right) \tag{37}$$

In this correlation T_u and P are unburned gas temperature and pressure during the combustion process. The reference parameters, 298 K and 1 atm respectively, represent the conditions at which the *unstretched* laminar flame velocity $S_{L,0}$ is calculated. α and β are functions of mixture equivalence ratio only. $S_{L,0}$ depends on type of fuel and, again, on equivalence ratio. A useful review of the most common correlations proposed in the literature can be found in Syed et al. [65]. For gasoline combustion in stoichiometric conditions the following constant values can be calculated: $\alpha = 2.129$; $\beta = -0.217$; $S_{L,0} = 0.28$ (m/s). Recent research work by Lindstrom et al. [50], Bayraktar [54] and by the Author [42], indicates that in the context of SI engine combustion, temperature and pressure exert weaker influences on the laminar flame speed (1.03 and -0.009 are the values of α and β , proposed for stoichiometric combustion in [50] to minimise the fitting errors of laminar speed functions to experimental combustion duration data). The presence of burned gas in the unburned mixture, as explained before, causes a substantial reduction in the flame velocity due to the reduction in heating value per unit of mass of the mixture. The fractional reduction in laminar speed, represented by the term $\left(1 - 2.06 x_b^{0.77}\right)$

originally proposed by Rhodes and Keck [58], has been found essentially independent of pressure, temperature, fuel type and equivalent ratio ϕ.

In [47], the exponential factors α and β are given the values 0.9 and -0.05, respectively; the unstretched laminar flame speed $S_{L,0}$ (units of m/s) is calculated through a modification of the functional expression proposed by Syed et al. [65], in which an increase of the ethanol volume fraction $\tilde{x}_{ETH}$ between 0% (pure gasoline) and 100% (pure ethanol) produces a 10% increase in laminar flame speed:

$$S_{L,0} = 0.4658 \ \left(1 + 0.1 \ \tilde{x}_{ETH}\right) \ \phi^{0.3} \ EXP\left(-4.48 \ \left(\phi - 1.075\right)^2\right) \tag{38}$$

5.2.3. Discussion of results

The flame propagation type models presented above are physics-based and hence, in principle, can be generalised to engines of different geometries. Through the definition of the laminar flame velocity, they enable accounting for two very relevant influences on combustion, i.e. the charge diluent fraction and the composition and strength of the fuel mixture. In spite of their simplicity, partly due to the range of assumptions taken, this type of control-oriented models has been demonstrated to capture the rate of combustion of modern SI engines with acceptable level of confidence. Hall et al. [47] validate the model using experimental records from a turbo-charged, PFI, flexible-fuel, SI engine, the specification of which are given in table 3.

Variable	Units	Values/Description
Test-engine configuration	-	In-line four-cylinder
Bore	mm	82.7
Stroke	mm	93.0
Connecting rod length	mm	144
Compression ratio	-	10.55
Total swept volume	cm^3	2100

Table 3. Specifications of the test engine used in reference [47].

More than 500 test points were used, consisting of combinations of engine speed between 750 and 5500 rev/min, intake manifold pressure between 0.4 and 2.2 bar, ST between -12 and 60 CA degrees BTDC and valve overlap between -16 and 24 CA degrees (intake valve timing only). Four basic ethanol/gasoline blend ratios were tested, between E0 (pure gasoline) and E85 (0.85 ethanol and 0.15 gasoline, as volume fractions). In the vast majority of instances, the model predicted the duration of the interval between ST and 50% MFB ($\Delta\vartheta_{50}$) with a maximum error of 10%. The influence of relevant engine parameters on combustion duration is summarized in figure 19. This shows the theoretical Spark Ignition Timing (SIT) which ensures

optimal 50% MFB location (i.e. at 8 CA degrees ATDC), when variable amounts of charge dilution (here Burned Gas Fraction), and variable amounts of ethanol are used, at different engine operating conditions. The $\Delta\vartheta_{50}$ interval can be evaluated indirectly, as the interval between SIT and 8 CA degrees ATDC.

As expected, an increase in the diluent fraction determines a slower combustion process (i.e. wider $\Delta\vartheta_{50}$) at all engine operating conditions, except at high engine load where the variation of the Burned Gas Fraction as a function of valve overlap is very limited. Conversely, the addition of ethanol to gasoline induces faster laminar flame speed and a stronger burning rate [65], reducing $\Delta\vartheta_{50}$ as a consequence. Increasing charge dilution necessitates more advanced theoretical ignition, whereas the ethanol content shows an opposite influence. An increase in dilution of 10 point percent requires about 25 CA degrees ignition advancement at low engine load. Increasing the ethanol content between E0 and E85 would reduce the required advancement between 3 and 6 CA degrees.

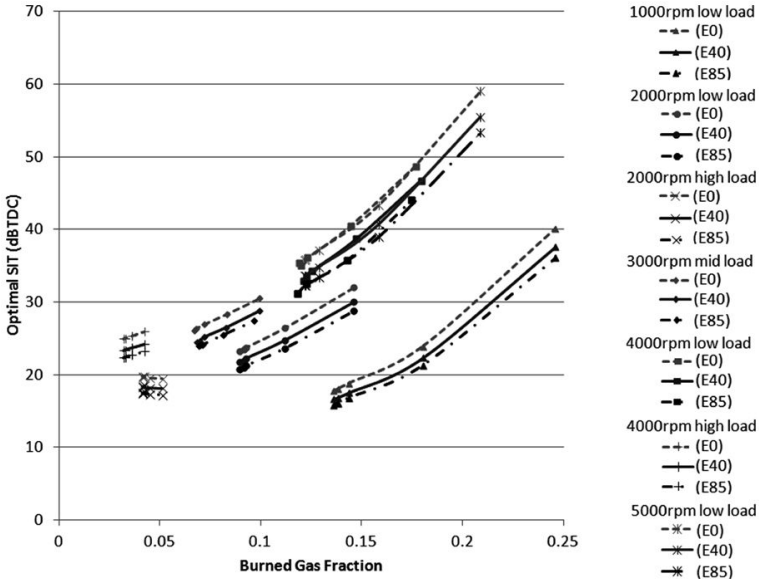

Figure 19. Spark ignition timing (SIT) required to locate the 50% MFB event at 8 CA degrees ATDC, and achieve optimal fuel efficiency, as a function of charge diluent fraction (Burned Gas Fraction), gasoline/ethanol blend ratio and engine speed/load operating conditions. Re-printed with permission by SAGE Publications from reference [47].

6. Conclusions

The present chapter explores the evolution of the combustion process in modern-design, premixed, gasoline engines, which feature the increasingly common technology of variable

valve timing. The assessment of combustion rates and duration has been performed by looking at the effects of a set of significant engine operating variables, which were studied in isolation. The chapter also explores recently-proposed simplified thermodynamic combustion models, which can be in principle deployed within fast-execution control algorithms. The engine data used cover a large portion of the part-load envelope, reflecting typical urban and cruise driving conditions, but incorporate high load operating conditions enabling a more comprehensive evaluation of combustion. The results presented are relevant to port-fuel injection gasoline engines, which feature homogeneous SI combustion, but also to direct-injection gasoline engines, because these run in theoretically-homogeneous combustion mode for a large part of the operating envelope. Despite burn rates and duration are invariably a function of engine geometry, the data used throughout the study for combustion analysis and modelling refer to the very common modern-design of 4-valve pent-roof combustion chamber, which also ascribes relevance and generality to the findings.

In modern engine architectures, the analysis of combustion tends to be intrinsically rich in details and challenging, and the ability to identify the most influential variables is crucial. Four operating variables are deemed as *essential and sufficient* to model the charge burn process in the context of current-design SI engines; in decreasing rank of importance these are charge dilution by burned gas, engine speed, ignition timing and charge density. In the present work dilution mass fraction, which slows the burning rate by increasing the cylinder charge heat capacity, has been of particular interest as large dilution variations produced by both valve timing setting and external-EGR are part of current combustion and emissions control strategies. The second most relevant engine variable is engine speed; greater engine speeds stretch the burning process over increasing intervals in the CA domain, as well as having a direct marked influence upon the level of combustion chamber turbulence. Similarly to engine load, the spark timing determines the thermodynamic state of the mixture when combustion commences, as well as controlling combustion phasing across TDC. Charge density calculated at spark timing is taken as an indication of engine load or of the amount of trapped mass within the cylinder.

Especially at low to medium load, the valve timing strategy exerts a strong influence upon both engine breathing ability and amount of burned gas internally recirculated during the valve overlap interval. Combustion control strategies aimed at improved efficiency must carefully consider the extent to which the burning characteristics are modified by VVT. Owing primarily to the influence of charge dilution, both FDA and RBA increase consistently with increasing degree of positive overlap, though the increase in RBA is more pronounced, and proportionately greater as engine load is reduced. In the range of valve timings investigated (EVC and IVO were varied between -14 and 36 and between -24 and 36 CA degrees BTDC, respectively), the experimental data show that the influence on combustion duration is exerted primarily through the overlap extension, whereas the overlap phasing about TDC is not critical. At relatively high load and speed conditions, combustion duration is found to be virtually independent of the valve timing setting. The effect of valve timing exerted through modifications to bulk motion and turbulence is not apparent in the data.

http://dx.doi.org/10.5772/55495

When the level of charge dilution is varied in isolation, by using fixed valve timing and variable amounts of external-EGR, both FDA and RBA increase linearly with increasing dilution, and the variation of RBA is slightly biased towards greater engine speed as a result of extending combustion further into the expansion stroke. When engine speed is varied in isolation, both combustion angles are found to increase linearly with increasing engine speed, with gradients of variation which appear independent of engine load. When engine speed increases between 1500 and 3000 rev/min, FDA and RBA grow by about 1/3 and 1/2, respectively.

Functional expressions for the total combustion angle, $\Delta\vartheta_{90}$, and the so-called form factor have been derived empirically as inputs of the Wiebe function to model the charge burn process of a premixed gasoline SI engine. The application of the model for $\Delta\vartheta_{90}$ yields average changes in the total burn angle of 10 CA degrees when dilution mass fraction increases by 5 point percent or engine speed increases by 800 rev/min. The maximum errors in FDA, RBA and $\Delta\vartheta_{50}$, calculated using the Wiebe function with modelled inputs, were within 13%, which is typical of simplified combustion models applied to complex engine architectures. Importantly, the analysis has shown that errors of magnitude up to 7% would be expected due to the inherent limitations of fitting a Wiebe function to an experimental MFB profile. The error analysis also shows that the influence of the Wiebe function form factor upon $\Delta\vartheta_{50}$ is relatively small, suggesting the modelling approach presented may be applicable to combustion phasing control.

Straightforward methods of combustion modelling as the Wiebe function or simplified flame propagation models (also outlined in this chapter) lend themselves ideally for robust inclusion into feed-back or feed-forward combustion control algorithms. If appropriately calibrated, these models are able to capture the most relevant factors influencing the rate of combustion and may enable efficiency improvement also during transient or variable operation. The main issue with the application of such models comes from relying on accurate values of in-cylinder charge dilution. High frequency sampling and analysis of the quantity of burned gas within the combustible mixture cannot be performed. Faster indirect measurement techniques are currently being studied, but are still far from becoming established technology. Engine mapping work may allow the compilation of multi-level look-up tables where dilution mass fraction can be tabulated as a function of engine speed, load, as well as intake and exhaust valve timing setting; these tables can be used to yield model inputs during steady-state running, less so during variable operation when the boundary conditions determining the diluent fraction change on a cycle-to-cycle basis. Physical measurements can be replaced by charge dilution models, but compounding the uncertainties associated to the various models may compromise the validity of the general approach. The best alternative among the various possible methods of combustion control would be the one enabling measurable improvements in fuel economy over a representative drive-cycle and further studies are needed in this field.

Supported by a vast and efficient infrastructure, the SI engine running on gasoline fuels continue to power the vast majority of light-duty vehicles used today across the globe. Due to the present level of technological advancement, as well as to the ever more stringent emission regulations, the homogenous premixed mode of combustion remains the favourite choice for

most production SI engines. The current scenario will not be altered easily, until new technologies and new alternative fuels become widely available and truly sustainable. In such a context, the investigation of gasoline premixed combustion, which in recent years is increasingly focusing on control strategy optimisation in *high-degree-of-freedom* engines, continues to be of paramount importance.

List of acronyms and abbreviations

ATDC	After Top Dead Centre
BDC	Bottom Dead Centre
BSFC	Brake Specific Fuel Consumption
BTDC	Before Top Dead Centre
CA	Crank Angle (degree)
COV	Coefficient Of Variability
E-EGR	External-Exhaust Gas Recirculation
EGR	Exhaust Gas Recirculation
EOC	End Of Combustion
EVC	Exhaust Valve Closing
EVO	Exhaust Valve Opening
FDA	Flame Development Angle
IC	Internal Combustion (Engine)
I-EGR	Internal-Exhaust Gas Recirculation
IMEP	Indicated Mean Effective Pressure
IVC	Inlet Valve Closing
IVO	Inlet Valve Opening
MBT	Maximum Brake Torque (Spark Timing)
MFB	Mass Fraction Burned
PFI	Port-Fuel Injection
RBA	Rapid Burning Angle
SI	Spark-Ignition
ST	Spark Timing
TDC	Top Dead Centre
TI-VVT	Twin Independent-Variable Valve Timing

http://dx.doi.org/10.5772/55495

VVA	Variable Valve Actuation
VVT	Variable Valve Timing – Variable Valve Phasing

List of main symbols

A	Average Flame Front Surface (m^2)
A / F	Air to Fuel Ratio
Δh	Combustion Chamber Mean Height (m)
m	Mass (m_b: Mass of Burned Gas; m_{tot}: Total In-Cylinder Trapped Mass) (kg)
$dm / d\tau$	Rate of Burning (kg/s)
n	Wiebe Function Form Factor or Polytropic Index
N	Engine Speed (rev/min)
P	In-Cylinder Pressure (ΔP: In-Cylinder Pressure Variation) (Pa)
S_L	Laminar Burning (or Flame Front) Velocity (S_b: Turbulent Velocity) (m/s)
S_P	Mean Piston Speed (m/s)
T	Temperature (K)
u'	In-Cylinder Turbulence Intensity (m/s)
V	In-Cylinder Volume (m^3)
γ	Ratio of Specific Heat Capacities
ϑ	Crank Angle Location (ϑ_{ST}: CA Location of Spark Ignition) (CA degrees)
$\Delta\vartheta$	Crank Angle Interval or Combustion Interval ($\Delta\vartheta_{50}$: Interval between ST and 50% MFB; $\Delta\vartheta_{90}$: Interval between ST and 90% MFB, Equal to FDA+RBA) (CA degrees)
ρ	Density (ρ_u: Density of the Unburned Charge; ρ_{ST}: In-Cylinder Density at Spark Timing) (kg/m^3)
τ	Instant of Time (s)
x	Mass Fraction (x_b: Total In-Cylinder Dilution Mass Fraction; x_{MFB}: Fresh Charge Burned Fraction)
$\bar{x}$	Molar or Volumetric Fraction

Author details

Fabrizio Bonatesta*

Department of Mechanical Engineering and Mathematical Sciences, Oxford Brookes University, Oxford, UK

References

[1] International Agency for Research on Cancer (IARC). Carcinogenicity of Diesel-Engine and Gasoline-Engine Exhausts and Some Nitroarenes. The Lancet Oncology 2012 13(7):663-664

[2] Yamin, J. A. A., Cupta, H. N., Bansal, B. B. and Srivastava, O. N. Effect of Combustion Duration on the Performance and Emission Characteristics of a Spark Ignition Engine Using Hydrogen as a Fuel. Int J Hydrogen Energy. 2005 25:581–589

[3] United States Environmental Protection Agency (EPA). Light-duty Automotive Technology, Carbon Dioxide Emissions, and Fuel Economy Trends 1975 through 2010. EPA-420-R-10-023. 2010 [Available online: http://www.epa.gov/otaq/cert/mpg/fetrends/420r10023.pdf]

[4] McAllister, S., Chen, J. and Fernandez-Pello, A. C. Premixed Piston IC Engines. Book chapter in: Fundamentals of Combustion Processes. Mechanical Engineering Series, 2011

[5] Prucka, R. G., Filipi, Z. S. and Assanis, D. N. Control-Oriented Model-Based Ignition Timing Prediction for High-Degrees-of-Freedom Spark Ignition Engines. Proc IMechE Part D: J Automobile Engineering 2012 226(6):828-839

[6] Heywood, J. B. Internal Combustion Engine Fundamentals. McGraw Hill, Automotive Technology Series, 1988

[7] Hicks, R. A., Lawes, M., Sheppard, C. G. W. and Whitaker, B. J. Multiple Laser Sheet Imaging Investigation of Turbulent Flame Structure in a Spark Ignition Engine. SAE Paper 941992, 1994

[8] Gillespie, L., Lawes, M., Sheppard, C. G. W. and Woolley, R. Aspects of Laminar and Turbulent Velocity Relevant to SI Engines. SAE Paper 2000-01-0192, 2000

[9] Keck, J. C. Turbulent Flame Structure and Speed in Spark-Ignition Engine. Proceedings of 19th Symposium (international) on Combustion, The Combustion Institute, 1982 (1451-1466)

[10] Keck, J. C., Heywood, J. B. and Noske, G. Early Flame Development and Burning Rates in Spark Ignition Engines and Their Cyclic Variability. SAE Paper 870164, 1987

[11] Beretta, G. P., Rashidi, M. and Keck, J. C. Turbulent Flame Propagation and Combustion in Spark Ignition Engines. Combustion and Flame 1983 52:217-245

[12] Groff, E.G. and Matekunas, F.A. The Nature of Turbulent Flame Propagation in a Homogeneous Spark Ignited Engine. SAE Paper 800133, 1980

[13] Rhodes, D. B. and Keck, J. C. Laminar Burning Speed Measurements of Indolene-Air-Diluent Mixtures at High Pressures and Temperatures. SAE Paper 850047, 1985

[14] Johansson, B. Influence of the Velocity Near the Spark Plug on Early Flame Development. SAE Paper 930481, 1993

[15] Kent, J. C., Mikulec, A., Rimal, L., Adamczyk, A. A., Stein, R. A. and Warren, C. C. Observation on the Effects of Intake-Generated Swirl and Tumble on Combustion Duration. SAE Paper 892096, 1989

[16] Newman, A. W., Girgis, N. S., Benjamin, S. F. and Baker, P. Barrel Swirl Behaviour in a Four-Valve Engine with Pent-roof Chamber. SAE Paper 950730, 1995

[17] Johansson, B. and Söderberg, F. The Effects of Valve Strategy on In-Cylinder Flow and Combustion. SAE Paper 960582, 1996

[18] Iguchi, S., Kudo, S., Furuno, S., Kashiwagura, T. and Yasui, T. Study of Mixture Formation and Gas Motion in an Internal Combustion Engine Using Laser Sheet 2-D Visualization. SAE Paper 885078, 1988

[19] Fraser, R. A. and Bracco, F. V. Cycle-Resolved LDV Integral Length Scale Measurements in an IC Engine. SAE Paper 880381, 1988

[20] Lancaster, D. R. Effects of Engine Variables on Turbulence in Spark-Ignition Engine. SAE Paper 760159, 1976

[21] Chen, C. and Veshagh, A. A Refinement of Flame Propagation Model for Spark-Ignition Engines. SAE Paper 920679, 1992

[22] Bonatesta, F. The Charge Burn Characteristics of a Gasoline Engine and the Influence of Valve Timing. PhD Thesis, University of Nottingham, UK, 2006.

[23] Hires, S. D., Tabaczynski, R. J. and Novak, J. M. The Prediction of Ignition Delay and Combustion Intervals for a Homogeneous Charge, Spark Ignition Engine. SAE Paper 780232, 1978

[24] Tabaczynski, R. J., Ferguson, C. R. and Radhakrishnan, K. A Turbulent Entrainment Model for Spark-Ignition Engine Combustion. SAE Paper 770647, 1977

[25] Wong, V. W. and Hoult, D. P. Rapid Distortion Theory Applied to Turbulent Combustion. SAE Paper 790357, 1979

[26] Alger, L. C. The Advantages and Control of Variable Valve Timing Under Part-Load Operating Conditions. PhD Thesis, The University of Nottingham, UK, 2005

[27] Jost, K. Spark Ignition Trends, Automotive Engineering International Magazine, January 2002, SAE International, Document number 1-110-1-26, 2002

[28] Ahmad, T. and Theobald, M. A Survey of Variable Valve Actuation Technology. SAE Paper 891674, 1989

[29] Tuttle, J. Controlling Engine Load by means of Early Intake Valve Closing. SAE Paper 820408, 1982

[30] Lenz, H., Wichart, K. and Gruden, D. Variable Valve Timing – A Possibility to Control Engine Load without Throttle. SAE Paper 880388, 1988

[31] Fontana, G., Galloni, E., Palmaccio, R. and Torella, E. The Influence of Variable Valve Timing on the Combustion Process of a Small Spark-Ignited Engine. SAE Paper 2006-01-0445, 2006.

[32] Cairns, A, Todd, A., Hoffman, H., Aleiferis, P. and Malcolm J. Combining Unthrottled Operation with Internal EGR Under Port and Central Direct Fuel Injection Conditions in a Single Cylinder SI Engine. SAE paper 2009-01-1835, 2009.

[33] Shayler, P. J. and Alger, L. C. Experimental Investigations of Intake and Exhaust Valve Timing Effects on Charge Dilution by Residuals, Fuel Consumption and Emissions at Part Load. SAE paper 2007-01-0478, 2007.

[34] Rassweiler, G. M. and Withrow, L. Motion Pictures of Engine Flame Propagation Model for S.I. Engines. SAE Journal (Trans.) 1938 42:185-204

[35] Shayler, P. J., Wiseman, M. W. and MA, T. Improving the Determination of Mass Fraction Burnt. SAE Paper 900351, 1990

[36] Amann, C. A. Cylinder Pressure Measurement and its Use in Engine Research. SAE Paper 852067, 1985

[37] Karim, G. A., Al-Alousi, Y. and Anson, W. Consideration of Ignition Lag and Combustion Time in a Spark Ignition Engine Using a Data Acquisition System. SAE Paper 820758, 1982

[38] Brunt, M. F. J. and Pond, C. R. Evaluation of Techniques for Absolute Cylinder Pressure Correction. SAE Paper 970036, 1997

[39] Payri, F., Molina, S., Martin, J. and Armas, O. Influence of Measurements Errors and Estimated Parameters on Combustion Diagnosis. Applied Thermal Engineering 2006 26:226-236

[40] Randolph, A. L. Methods of Processing Cylinder-Pressure Transducer Signals to Maximize Data Accuracy. SAE Paper 900170, 1990

[41] Brunt, M. F. J. and Emtage, A. L. Evaluation of Burn Rate Routines and Analysis Errors. SAE Paper 970037, 1997

[42] Bonatesta, F. and Shayler, P. J. Factors Influencing the Burn Rate Characteristics of a Spark Ignition Engine with Variable Valve Timing. Proc IMechE Part D: J Automo-

bile Engineering, 2008 222(11):2147–2158. The final, definitive version of this paper has been published by SAGE Publications Ltd, All rights reserved © [Available online: http://online.sagepub.com]

[43] Bozza, F., Gimelli, A., Senatore, A. and Caraceni, A. A Theoretical Comparison of Various VVA Systems for Performance and Emission Improvements of S.I. Engines. SAE Paper 2001-01-0670, 2001

[44] Sandquist, H., Wallesten, J., Enwald, K. and Stromberg, S. Influence of Valve Overlap Strategies on Residual Gas Fraction and Combustion in a Spark-Ignition Engine at Idle. SAE Paper 972936, 1997

[45] Scharrer, O., Heinrich, C., Heinrich, M., Gebhard, P. And Pucher, H. Predictive Engine Part Load Modeling for the Development of a Double Variable Cam Phasing (DVCP) Strategy. SAE Paper 2004-01-0614, 2004

[46] Bonatesta, F., Waters, B. and Shayler, P. J. Burn Angles and Form Factors for Wiebe Function Fits to Mass Fraction Burned Curves of a Spark-Ignition Engine with Variable Valve Timing. Int J Engine Res 2010 11(2):177–186. The final, definitive version of this paper has been published by SAGE Publications Ltd, All rights reserved © [Available online: http://online.sagepub.com]

[47] Hall, C. M., Shaver, G. M., Chauvin, J. and Petit, N. Control-Oriented Modelling of Combustion Phasing for a Fuel-Flexible Spark-Ignited Engine with Variable Valve Timing. Int J Engine Res 2012 13(5):448–463.

[48] Ghojel, J. I. Review of the Development and Applications of the Wiebe Function: A Tribute to the Contribution of Ivan Wiebe to Engine Research. Int J Engine Res 2010 11(4):297-312

[49] Oppenheim, A. K. and Kuhl, A. L. Life of Fuel in a Cylinder. SAE Paper 980780, 1998

[50] Lindström, F., Angstrom, H., Kalghati, G. and Moller, C. An Empirical S.I. Combustion Model Using Laminar Burning Velocity Correlations. SAE Paper 2005-01-2106, 2005

[51] Soylu, S. and Van Gerpen, J. Development of Empirically Based Burning Rate Sub-Models for a Natural Gas Engine. Energy Conversion and Management 2004 45:467–481

[52] Csallner, P. Eine Methode zur Vorausberechnung des Brennverlaufs von Ottomotoren bei geanderten Betriebsdedingungen. Dissertation, TU Munchen, 1981

[53] Witt, A. Analyse der Thermodynamischen Verluste eines Ottomotors Unter den Randbedingungen Variber Steuerzeiten. Dissertation, Graz Techn. University, 1999

[54] Bayraktar, H. and Durgun, O. Development of an Empirical Correlation for Combustion Durations in Spark Ignition Engines. Energy Conversion and Management 2004 45:1419–1431.

[55] Vávra, J. and Takáts, M. Heat Release Regression Model for Gas Fuelled SI Engines. SAE Paper 2004-01-1462, 2004

[56] Galindo, J., Climent, H., Plá, B. and Jiménez, V. D. Correlations for Wiebe Function Parameters for Combustion Simulation in Two-Stroke Small Engines. Applied Thermal Engineering 2011 31:1190–1199

[57] Prucka, R., Lee, T., Filipi, Z., and Assanis, D. Turbulence Intensity Calculation from Cylinder Pressure Data in a High Degree of Freedom Spark-Ignition Engine. SAE Paper 2010-01-0175, 2010

[58] Rhodes, D. B. and Keck, J. C. Laminar Burning Speed Measurements of Indolene-Air-Diluent Mixtures at High Pressures and Temperatures. SAE Paper 850047, 1985

[59] Metghalchi, M. and Keck, J. C. Burning Velocities of Air with Methanol, Isooctane and Indolene at High Pressure and Temperature. Combustion and Flame 1982 48:191-210

[60] Chen, C. and Veshagh, A. A Refinement of Flame Propagation Combustion Model for Spark-Ignition Engines. SAE Paper 920679, 1992

[61] Blizard, N. and Keck, J. Experimental and Theoretical Investigation of Turbulent Burning Model for Internal Combustion Engines. SAE Paper 740191, 1974

[62] Stone, R. Introduction to Internal Combustion Engines. MACMILLAN PRESS LTD, Third Edition, 1999

[63] Bradley, D., Gaskell, P. H. and Gu, X. J. Burning Velocities, Markstein Lengths and Flame Quenching for Spherical Methane-Air Flames: a Computational Study. Combustion and Flame 1996 104:176-198

[64] Turns, S. R. An Introduction to Combustion; Concepts and Applications, McGraw Hill Book Company, Mechanical Engineering Series, Second Edition, 2000

[65] Syed, I., Yeliana, Y., Mukherjee, A., Naber, J. and Michalek, D. Numerical Investigation of Laminar Flame Speed of Gasoline - Ethanol/Air Mixtures with Varying Pressure, Temperature and Dilution. SAE Paper 2010-01-0620, 2010